PERIÓDICO TCHÊ QUÍMICA
ARTIGO ORIGINAL

SÍNTESE, CARACTERIZAÇÃO ESPECTROSCÓPICA E DOCKING MOLECULAR DE NOVOS HÍBRIDOS DE 1,4-DI-HIDROPIRIDINA–1,2,4-TRIAZOLIDINA-3-TIONA CONTRA A TIROSINA QUINASE EGFR

SYNTHESIS, SPECTROSCOPIC CHARACTERIZATION, AND MOLECULAR DOCKING OF NOVEL 1,4-DIHYDROPYRIDINE–1,2,4-TRIAZOLIDINE-3-THIONE HYBRIDS AGAINST EGFR TYROSINE KINASE

تخليق وتوصيف طيفي والتحام جزيئي لمركبات هجينة جديدة من 1،4--ثنائي هيدروبيريدين1،2،4-تريازوليدين-3-ثيون تجاه إنزيم تيروسين كيناز لمستقبل عامل نمو البشرة(EGFR)

Maryam Sabri Hashim*
Department of Chemistry, College of Science, University of Misan, Misan, Iraq.
ORCID: https://orcid.org/0009-0004-5597-3691

Tahseen Saddam Fandi Al-Mathkuri
Department of Chemistry, College of Science, University of Misan, Misan, Iraq.
ORCID: https://orcid.org/0000-0002-6234-0137

** Corresponding author*
e-mail: mariam19@uomisan.edu.iq

Received 12 January 2026; received in revised form 20 April 2026; accepted 20 June 2026

RESUMO

Introdução: Sistemas heterocíclicos híbridos que combinam núcleos estruturalmente e farmacologicamente relevantes são de interesse em química medicinal, pois a integração de diferentes arcabouços pode ampliar a diversidade molecular e modificar o comportamento de ligação ao alvo. **Objetivo:** Sintetizar e caracterizar estruturalmente uma nova série de híbridos 1,4-di-hidropiridina–1,2,4-triazolidina-3-tiona e investigar suas interações previstas com o domínio tirosina-quinase do receptor do fator de crescimento epidérmico (EGFR). **Métodos:** Os compostos-alvo foram preparados por uma sequência de três etapas: condensação multicomponente do tipo Hantzsch, formilação de Vilsmeier–Haack e ciclização com tiosemicarbazida. Os intermediários e produtos finais foram caracterizados por espectroscopia no infravermelho com transformada de Fourier (FT-IR), ressonância magnética nuclear (RMN) de ^{1}H e ^{13}C, Distortionless Enhancement by Polarization Transfer (DEPT-135) e espectrometria de massas. O docking molecular foi realizado contra o domínio tirosina-quinase do EGFR obtido do Protein Data Bank (PDB ID: 6JWL), utilizando o software Molecular Operating Environment. **Resultados:** Os derivados-alvo foram obtidos com rendimentos moderados a bons, e os dados espectroscópicos foram consistentes com as estruturas propostas. Entre os compostos submetidos ao docking, M9 apresentou o escore previsto mais favorável (–15,91 kcal/mol), seguido por M6, M3 e M12 (–14,64, –14,49 e –14,44 kcal/mol, respectivamente). As poses previstas mostraram interações com resíduos do sítio ativo do EGFR, incluindo Lys745, Thr790 e Asp855. **Discussão:** As diferenças no comportamento de ligação previsto foram associadas à natureza e à posição dos substituintes arila. O derivado para-cloro M9 apresentou o escore de docking mais favorável nas condições computacionais aplicadas. **Conclusões:** Uma nova série de híbridos 1,4-di-hidropiridina–1,2,4-triazolidina-3-tiona foi sintetizada e caracterizada. M9 foi o candidato computacional mais bem classificado; entretanto, os resultados são preliminares e requerem confirmação por ensaios in vitro de inibição do EGFR, citotoxicidade e seletividade.

Palavras-chave: *1,4-di-hidropiridina; 1,2,4-triazolidina-3-tiona; híbridos heterocíclicos; reação de Vilsmeier–Haack; docking molecular; tirosina quinase EGFR; caracterização espectroscópica.*

ABSTRACT

Background: Hybrid heterocyclic systems that combine structurally and pharmacologically relevant scaffolds are of interest in medicinal chemistry because scaffold integration can expand molecular diversity and alter target-binding behavior. **Aim:** To synthesize and structurally characterize a new series of 1,4-dihydropyridine–1,2,4-triazolidine-3-thione hybrids and investigate their predicted interactions with the epidermal growth factor receptor (EGFR) tyrosine kinase domain. **Methods:** The target compounds were prepared through a three-step sequence involving Hantzsch-type multicomponent condensation, Vilsmeier–Haack formylation, and cyclization

DOI: 10.52571/PTQ.v23.n53.2026_07_SABRI_pgs_76_115.pdf

with thiosemicarbazide. Intermediates and final products were characterized by Fourier-transform infrared (FT-IR) spectroscopy, proton and carbon-13 nuclear magnetic resonance (^{1}H-NMR and ^{13}C-NMR), Distortionless Enhancement by Polarization Transfer (DEPT-135), and mass spectrometry. Molecular docking was performed against the EGFR tyrosine kinase domain obtained from the Protein Data Bank (PDB ID: 6JWL) using Molecular Operating Environment software. **Results:** The target derivatives were obtained in moderate to good yields, and the spectroscopic data were consistent with the proposed structures. Among the docked compounds, M9 showed the most favorable predicted docking score (−15.91 kcal/mol), followed by M6, M3, and M12 (−14.64, −14.49, and −14.44 kcal/mol, respectively). The predicted poses showed interactions with EGFR active-site residues, including Lys745, Thr790, and Asp855. **Discussion:** Differences in predicted binding behavior were associated with the nature and position of the aryl substituents. The para-chloro derivative M9 showed the most favorable docking score under the applied computational conditions. **Conclusions:** A new series of 1,4-dihydropyridine–1,2,4-triazolidine-3-thione hybrids was synthesized and structurally characterized. M9 was the highest-ranked computational candidate; however, the findings are preliminary and require confirmation through in vitro EGFR-inhibition, cytotoxicity, and selectivity studies.

Keywords*: 1,4-Dihydropyridine; 1,2,4-triazolidine-3-thione; heterocyclic hybrids; Vilsmeier–Haack reaction; molecular docking; EGFR tyrosine kinase; spectroscopic characterization.*

الملخص

الخلفية: تحظى الأنظمة الحلقية غير المتجانسة الهجينة، التي تجمع بين هياكل بنائية ذات أهمية دوائية، باهتمام في الكيمياء الطبية؛ إذ يمكن أن يؤدي الدمج الهيكلي إلى تعزيز التنوع الجزيئي وتعديل سلوك الارتباط بالأهداف البيولوجية. **الهدف:** تخليق وتوصيف سلسلة جديدة من المركبات الهجينة التي تجمع بين نواة 1،4-ثنائي هيدروبيريدين ونواة 1،2،4-تريازوليدين-3-ثيون، ودراسة تفاعلاتها المتوقعة مع نطاق إنزيم تيروسين كيناز لمستقبل عامل نمو البشرة (EGFR). **طرائق العمل:** حُضّرت المركبات المستهدفة عبر ثلاث خطوات شملت تكاثف هانتزش متعدد المكونات، وفورملة فيلسمير–هاك، والإغلاق الحلقي باستخدام الثيوسيميكاربازيد. وجرى توصيف المركبات الوسيطة والنهائية بمطيافية الأشعة تحت الحمراء بتحويل فورييه(FT-IR) ، ومطيافية الرنين المغناطيسي النووي (NMR) للبروتون والكربون ^{1}H-NMR) 13-و^{13}C-NMR)، وتقنية تعزيز الاستقطاب عديم التشوه(DEPT-135) ، ومطيافية الكتلة. وأُجري الالتحام الجزيئي مع نطاق تيروسين كيناز لمستقبل EGFR المأخوذ من بنك بيانات البروتين (PDB ID: 6JWL) باستخدام برنامج Molecular Operating Environment. **النتائج:** تم الحصول على المشتقات المستهدفة بنواتج متوسطة إلى جيدة، وكانت البيانات الطيفية متوافقة مع التراكيب المقترحة. وأظهر المركب M9 أفضل درجة التحام متوقعة 15.91− كيلو كالوري/مول(، تلاه M6 و M3و 14.64−) M12و 14.49−و 14.44−كيلو كالوري/مول، على التوالي. (وأظهرت أوضاع الالتحام المتوقعة تفاعلات مع بقايا في الموقع النشط لمستقبلEGFR ، منها Lys745 و Thr790 و Asp855. **المناقشة:** ارتبطت الاختلافات في سلوك الارتباط المتوقع بطبيعة مستبدلات الأريل وموقعها، وكان مشتق البارا-كلورو M9 صاحب أفضل درجة التحام ضمن الظروف الحسابية المطبقة. **الاستنتاجات:** تم تخليق وتوصيف سلسلة جديدة من هجائن1 ،-4ثنائي هيدروبيريدين1−،2،-4تريازوليدين-3-ثيون. وكان M9 المرشح الحسابي الأعلى ترتيباً؛ إلا أن النتائج أولية وتتطلب تأكيداً باختبارات تثبيط EGFR والسمية الخلوية والانتقائية في المختبر.

الكلمات المفتاحية: *1،4-ثنائي هيدروبيريدين1،2،4-تريازوليدين-3-ثيون ؛ هجائن حلقية غير متجانسة؛ تفاعل فيلسمير–هاك؛ الالتحام الجزيئي؛ تيروسين كيناز مستقبل عامل نمو البشرة(EGFR) ؛ التوصيف الطيفي.*

1. INTRODUCTION

Heterocyclic compounds are organic cyclic systems containing at least one heteroatom within the ring structure. The most common heteroatoms are nitrogen, oxygen, and sulfur; however, heterocycles incorporating other elements, such as selenium (Abdel-Hafez, 2008), phosphorus, iron, and magnesium, have also been reported. These compounds represent one of the most prevalent and significant classes in organic chemistry, accounting for nearly half of the approximately 50 million organic compounds documented in the Chemical Abstracts database (Comins and Ma, 2016).

The importance of heterocyclic compounds arises from their broad biological and pharmacological relevance. They are key structural components of many pharmaceuticals, natural products, and biomolecules. In oncology, nitrogen-containing heterocycles are especially important because they provide scaffolds for kinase-targeted agents, including inhibitors of epidermal growth factor receptor (EGFR) signaling (Vitaku, Smith, and Njardarson, 2014; Irfan *et al.*, 2025). Structurally, heterocycles are broadly classified into aromatic (Zhao *et al.*, 2017) and non-aromatic systems (Vitaku, Smith, and Njardarson, 2014). Many biologically active compounds contain five- or six-membered rings bearing one to three heteroatoms, either as isolated rings or fused systems such as the purine and pyrimidine bases in DNA (Kabir and Uzzaman, 2022). The clinical and pharmacological relevance of mutant-selective EGFR inhibition is exemplified by osimertinib, a third-generation irreversible inhibitor developed for sensitizing and T790M-resistant EGFR variants (Cross *et al.*, 2014).

Among heterocyclic systems, the pyridine ring has attracted considerable attention due to its versatile applications in medicinal and materials chemistry. Partial or complete reduction

of pyridine yields important derivatives such as piperidine, tetrahydropyridines, and dihydropyridines, each possessing distinct chemical and pharmacological properties. Notably, more than 85% of biologically active compounds either contain heterocyclic rings or are entirely heterocyclic in nature (Heravi, 2020), with representative examples including milrinone and amrinone (Chalán-Gualán *et al*., 2022).

In particular, the 1,4-dihydropyridine ring is a six-membered heterocyclic system containing one nitrogen atom (Hussein and Al-Mathkuri, 2025) and is considered a crucial scaffold in medicinal chemistry. Its derivatives exhibit a wide spectrum of pharmacological activities, making them essential frameworks in drug design. Extensive research has demonstrated that dihydropyridine derivatives can interact with multiple biological targets, highlighting their therapeutic potential and importance in the development of modern pharmaceuticals (Ali and Al-Mathkuri, 2023).

Despite substantial progress in this field, structural modification of dihydropyridine systems to improve target engagement remains an active area of research (Lago *et al*., 2023). One strategy is to incorporate an additional heterocyclic moiety into a dihydropyridine or dihydropyridinone core to expand chemical space and modulate target specificity (Faizan *et al*., 2024). Thiosemicarbazone derivatives and their cyclized 1,2,4-triazolidine-3-thione products are attractive in this context because of their versatile reactivity and medicinal-chemistry relevance (Gričar *et al*., 2025). However, their integration with dihydropyridinone scaffolds remains insufficiently explored. Recent analyses of catalytic 1,4-dihydropyridine synthesis further emphasize continued efforts to improve efficiency, sustainability, and structural diversity in this scaffold class (Soni *et al*., 2025).

Although 1,4-dihydropyridine derivatives and 1,2,4-triazolidine-3-thione systems have each been investigated because of their pharmacological relevance, comparatively little attention has been given to hybrid structures that combine both motifs within one molecular framework; previous studies have mainly examined independently substituted dihydropyridines, thiosemicarbazones, or triazolidine derivatives (Patil *et al*., 2019; Ramesh and Lalitha, 2016). The direct construction of 1,4-dihydropyridine–1,2,4-triazolidine-3-thione hybrids, particularly the effect of electron-withdrawing aryl substituents on synthesis, spectroscopic features, and predicted EGFR binding, therefore represents a defined research gap.

In the present work, a new series of 1,4-dihydropyridine derivatives bearing a 1,2,4-triazolidine-3-thione moiety was synthesized through a sequential three-step route involving Hantzsch condensation, Vilsmeier–Haack formylation, and cyclization with thiosemicarbazide. The compounds contained p-NO_2, p-Br, p-Cl, or o-Cl aryl substituents to examine their effects on reaction yield, spectroscopic behavior, and predicted molecular interactions. Molecular docking against the EGFR tyrosine kinase domain was used as a preliminary computational approach, consistent with prior EGFR-focused studies of dihydropyridine derivatives (Mansour *et al*., 2022; Faizan *et al*., 2024).

1.1. Aims

The main aim of this study was to synthesize and structurally characterize a new series of 1,4-dihydropyridine–1,2,4-triazolidine-3-thione hybrid derivatives and to investigate their predicted interactions with the EGFR tyrosine kinase domain using molecular docking.

The specific objectives were:

1. To prepare substituted 1,4,5,6-tetrahydropyridine derivatives through a Hantzsch-type multicomponent reaction.
2. To convert the synthesized intermediates into 5-formyl-1,4-dihydropyridine derivatives using Vilsmeier–Haack formylation.
3. To synthesize the corresponding 1,2,4-triazolidine-3-thione derivatives by reaction with thiosemicarbazide.
4. To characterize the synthesized compounds using FT-IR, ^{1}H NMR, ^{13}C NMR, DEPT-135, and mass spectrometry.
5. To examine the influence of p-NO_2, p-Br, p-Cl, and o-Cl substituents on the synthetic yields and spectroscopic behavior of the compounds.
6. To evaluate the predicted binding modes and interaction profiles of the final derivatives within the EGFR tyrosine kinase active site.

2. MATERIALS AND METHODS

2.1. Materials

All chemicals and solvents used in this study were of analytical grade and were obtained from commercial suppliers, including Merck, BDH, and Sigma-Aldrich. The reagents included 4-nitrobenzaldehyde, 4-bromobenzaldehyde, 4-chlorobenzaldehyde, 2-chlorobenzaldehyde, Meldrum's acid, methyl acetoacetate, ammonium acetate, glacial acetic acid, dimethylformamide (DMF), phosphorus oxychloride ($POCl_3$), thiosemicarbazide, sodium acetate, and anhydrous sodium sulfate. The solvents used included dichloromethane, ethanol, methanol, ethyl acetate, petroleum ether, and distilled water. Silica gel was used for column chromatography, and pre-coated silica gel 60 F_{254} plates were used for thin-layer chromatography. Unless otherwise stated, all chemicals were used without further purification.

2.2. Instrumentation

Reaction progress was monitored by thin-layer chromatography (TLC) on pre-coated silica gel 60 F_{254} plates, and spots were visualized under ultraviolet light. Column chromatography was performed using 60–120-mesh silica gel. Melting points were measured on a Stuart SMP11 apparatus and are uncorrected. Fourier-transform infrared (FT-IR) spectra were recorded on a Shimadzu IR Affinity-1 spectrophotometer using KBr pellets over 4000–400 cm^{-1}. Proton and carbon-13 nuclear magnetic resonance (^1H NMR and ^{13}C NMR) spectra, including Distortionless Enhancement by Polarization Transfer (DEPT-135) experiments, were acquired on a Bruker spectrometer at 400 MHz for ^1H and 101 MHz for ^{13}C. $CDCl_3$ and DMSO-d_6 were used as deuterated solvents, with tetramethylsilane as the internal reference. Electrospray-ionization mass spectra were recorded on an AB SCIEX 3200 QTRAP instrument. Molecular structures and docking simulations were prepared and analyzed using Molecular Operating Environment (MOE), version 2014.

2.3. Methods

2.3.1. Synthesis of methyl 2-methyl-4-(substituted phenyl)-6-oxo-1,4,5,6-tetrahydropyridine-3-carboxylate derivatives (M1, M4, M7, and M10)

The synthesis was performed using a Hantzsch-type multicomponent procedure adapted from Vijesh *et al.* (2011). Methyl acetoacetate (1 mmol), the appropriate substituted benzaldehyde (1 mmol), Meldrum's acid (1 mmol), and ammonium acetate (1.5 mmol) were dissolved in glacial acetic acid (10 mL). The reaction mixture was heated under reflux at 120 °C for 12 h, as shown in Equation 1. Reaction progress was monitored by TLC using ethyl acetate/petroleum ether (1:3, v/v) as the mobile phase.

After completion, the reaction mixture was cooled to room temperature. For the 4-bromo, 4-chloro, and 2-chloro derivatives, the precipitated solids were collected by filtration, washed with cold ethanol, and recrystallized from methanol.

For the 4-nitro derivative, no precipitate formed upon cooling. The solvent was removed under reduced pressure, and the crude product was purified by column chromatography using ethyl acetate/petroleum ether. The isolated product was dried and characterized by FT-IR, ^1H NMR, ^{13}C NMR, and DEPT-135 spectroscopy.

2.3.2. Synthesis of methyl 6-chloro-4-(substituted phenyl)-5-formyl-2-methyl-1,4-dihydropyridine-3-carboxylate derivatives (M2, M5, M8, and M11)

The Vilsmeier–Haack formylation was performed using a procedure adapted from Armas *et al.* (2000). Dimethylformamide (1.24 mL, 16 mmol) in dichloromethane (4 mL) was added dropwise to phosphorus oxychloride (1.5 mL, 16 mmol) with continuous stirring at room temperature. The mixture was stirred for 30 min to generate the Vilsmeier–Haack reagent.

A solution of the appropriate methyl 2-methyl-4-(substituted phenyl)-6-oxo-1,4,5,6-tetrahydropyridine-3-carboxylate derivative (4 mmol) in dichloromethane (16 mL) was then added slowly. The resulting reaction mixture was stirred at room temperature for 24 h, as shown in Equation 2. Reaction progress was monitored by thin-layer chromatography using ethyl acetate/petroleum ether (1:2, v/v).

After completion, an aqueous sodium acetate solution, prepared by dissolving 16 g of sodium acetate in 24 mL of distilled water, was added slowly over 1 h with continuous stirring. The mixture was extracted three times with dichloromethane, and the combined organic layers were dried over anhydrous sodium sulfate. The solvent was removed under reduced pressure.

The crude products were purified by column chromatography using ethyl acetate/petroleum ether (1:6, v/v) as the eluent. The purified derivatives were obtained as light-

yellow or yellow solids and were characterized by FT-IR, ^{1}H NMR, and ^{13}C NMR spectroscopy.

2.3.3. Synthesis of methyl 6-chloro-4-(substituted phenyl)-2-methyl-5-(5-thioxo-1,2,4-triazolidin-3-yl)-1,4-dihydropyridine-3-carboxylate derivatives (M3, M6, M9, and M12)

The cyclization procedure was adapted from reported thiosemicarbazone-to-triazolidine-3-thione transformations (Gričar *et al.*, 2025; Patil *et al.*, 2019; Ramesh and Lalitha, 2016). Thiosemicarbazide (1 mmol) and the appropriate methyl 6-chloro-4-(substituted phenyl)-5-formyl-2-methyl-1,4-dihydropyridine-3-carboxylate derivative (1 mmol) were dissolved in ethanol (5 mL) and distilled water (15 mL). The reaction mixture was heated under reflux at 80 °C for 12 h with continuous stirring, as shown in Equation 3.

Reaction progress was monitored by thin-layer chromatography using ethyl acetate/petroleum ether (1:3, v/v). After completion, the mixture was cooled to room temperature, and the resulting precipitate was collected by filtration, washed with cold ethanol, and dried.

The crude products were purified by column chromatography using ethyl acetate/petroleum ether (1:6, v/v) as the eluent. FT-IR, ^{1}H-NMR, ^{13}C-NMR, and mass spectrometry were used to characterize the purified final compounds.

2.4. Molecular Docking Study

Molecular docking was conducted to examine the predicted binding modes of M3, M6, M9, and M12 within the EGFR tyrosine kinase domain, following a workflow comparable to that used for dihydropyridine-based EGFR ligands (Mansour *et al.*, 2022). The crystal structure of the L858R-mutant EGFR kinase domain in complex with osimertinib (AZD9291) was obtained from the Protein Data Bank (PDB ID: 6JWL; 2.55 Å resolution); the co-crystallized ligand is identified as YY3. The Protein Data Bank is the principal open repository for experimentally determined three-dimensional macromolecular structures (Burley *et al.*, 2019).

The receptor was prepared in MOE version 2014 by inspecting structural inconsistencies, removing water and non-essential crystallographic species, adding hydrogen atoms, assigning protonation states under physiological conditions, and minimizing the structure while preserving the crystallographic geometry. The co-crystallized osimertinib molecule was retained to define the ATP-binding site and validate the protocol, then removed before docking the synthesized compounds. Ligands M3, M6, M9, and M12 were constructed, protonated, and energy-minimized in MOE.

The active site was defined from the position of co-crystallized osimertinib. Ligands were placed using Triangle Matcher, initially scored with London dG, and the 30 highest-ranked poses were subjected to rigid-receptor refinement and rescoring with GBVI/WSA dG. The five highest-ranked refined poses were retained for each ligand.

Protocol validation was performed by redocking co-crystallized osimertinib under the same placement, scoring, and refinement settings. Reproduction of the crystallographic orientation was assessed using the heavy-atom root-mean-square deviation (RMSD), with a predefined acceptance criterion of RMSD ≤ 2.0 Å. This cutoff is consistent with the commonly applied criterion for successful reproduction of crystallographic ligand poses in docking-validation studies (Warren *et al.*, 2006; Goullieux *et al.*, 2023).

The final poses of the synthesized compounds and reference ligand were evaluated using the GBVI/WSA dG score, pose RMSD, orientation in the ATP-binding pocket, hydrogen-bond interactions, and other polar or hydrophobic contacts with active-site residues.

3. RESULTS AND DISCUSSION

3.1. Results

The synthesized compounds (M1–M12) were obtained successfully. Their physical characteristics (color and melting point), reaction yields, molecular formulae, and chemical structures are summarized in Table 1.

3.1.1. Spectroscopic Characterization of 1,4,5,6-Tetrahydropyridine Derivatives (M1, M4, M7, and M10)

3.1.1.1. Methyl 2-methyl-4-(4-nitrophenyl)-6-oxo-1,4,5,6-tetrahydropyridine-3-carboxylate (M1)

Off-white; yield = 41%; m.p. = 202 °C (Table 1). FT-IR (KBr, vmax, cm^{-1}): 3466–3416 (N–H), 3116 (Ar–H), 2947 (aliphatic C–H), 1793 (C=O, ester), 1699 (C=O, amide), 1637–1599 (C=C, aromatic/olefinic), 1514 (NO_2, asym), 1350 (NO_2, sym), 1489–1450 (C–C, aliphatic), 1284 (C–N, NO_2), 1201 (C–N, amide), 1178, 1109, 1085 (C–O, ester), 854–833 (Ar–C–H, out-of-plane). ^{1}H NMR (400 MHz, DMSO-d_6) δ 10.06 (s, 1H, NH),

8.16 (d, J = 8.7 Hz, 2H, Ar–H), 7.43 (d, J = 8.6 Hz, 2H, Ar–H), 4.27 (d, J = 7.5 Hz, 1H, CH), 3.53 (s, 3H, OCH_3), 3.03 (dd, J = 16.4, 7.5 Hz, 1H, CH_2), 2.44 (d, J = 16.2 Hz, 1H, CH_2), 2.35 (s, 3H, CH_3). ^{13}C NMR (101 MHz, DMSO-d_6) δ 169.27, 166.73, 150.65, 149.57, 146.43, 128.04, 123.91, 103.49, 51.18, 39.52, 37.91, 37.40, 18.33.

3.1.1.2. Methyl 4-(4-bromophenyl)-2-methyl-6-oxo-1,4,5,6-tetrahydropyridine-3-carboxylate (M4)

Off-white; yield = 44.4%; Rf = 0.65; m.p. = 187 °C (Table 1). FT-IR (KBr, vmax, cm^{-1}): 3464 (N–H), 3057 (Ar–H), 2951 (aliphatic C–H), 1708 (C=O, ester), 1689 (C=O, lactam), 1631 (C=C, DHP ring), 1539 (Ar C=C), 1489 (C=C), 1311 (C–N), 1226 (C–O), 1085 (C–O–C), 731 (Ar–H, out-of-plane), 630 (C–Br). ^{1}H NMR (400 MHz, $CDCl_3$) δ 8.47 (s, 1H, NH), 7.42 (d, J = 8.2 Hz, 2H, Ar–H), 7.07 (d, J = 8.2 Hz, 2H, Ar–H), 4.23 (d, J = 7.9 Hz, 1H, CH), 3.67 (s, 3H, OCH_3), 2.91 (dd, J = 16.5, 7.9 Hz, 1H, CH_2), 2.64 (d, J = 16.5 Hz, 1H, CH_2), 2.40 (s, 3H, CH_3). ^{13}C NMR (101 MHz, $CDCl_3$) δ 170.54, 167.06, 146.54, 140.97, 131.90, 128.46, 120.87, 106.68, 51.41, 37.89, 37.43, 19.14.

3.1.1.3. Methyl 4-(4-chlorophenyl)-2-methyl-6-oxo-1,4,5,6-tetrahydropyridine-3-carboxylate (M7)

Off-white; yield = 30%; Rf = 0.67; m.p. = 173 °C (Table 1). FT-IR (KBr, vmax, cm^{-1}): 3475 (N–H), 3124 (Ar–H), 2947 (aliphatic C–H), 1747 (C=O, ester), 1697 (C=O, lactam), 1633 (C=C, DHP ring), 1558 (Ar C=C), 1489 (C=C), 1313 (C–N), 1222 (C–O), 1082 (C–O–C), 823 (Ar–H, out-of-plane), 651 (C–Cl). ^{1}H NMR (400 MHz, $CDCl_3$) δ 8.44 (s, 1H, NH), 7.24 (d, J = 8.4 Hz, 2H, Ar–H), 7.12 (d, J = 8.3 Hz, 2H, Ar–H), 4.22 (d, J = 7.7 Hz, 1H, CH), 3.68 (s, 3H, OCH_3), 2.92 (dd, J = 16.5, 7.7 Hz, 1H, CH_2), 2.64 (d, J = 16.5 Hz, 1H, CH_2), 2.43 (s, 3H, CH_3). ^{13}C NMR (101 MHz, $CDCl_3$) δ 170.85, 167.15, 146.72, 140.32, 132.80, 128.97, 128.12, 106.67, 51.56, 38.03, 37.26, 19.20.

3.1.1.4. Methyl 4-(2-chlorophenyl)-2-methyl-6-oxo-1,4,5,6-tetrahydropyridine-3-carboxylate (M10)

Off-white; yield = 42%; Rf = 0.67; m.p. = 195 °C (Table 1). FT-IR (KBr, vmax, cm^{-1}): 3477 (N–H), 3057 (Ar–H), 2954 (aliphatic C–H), 1707 (C=O, ester), 1633 (C=C, DHP ring), 1539 (Ar C=C), 1487 (C=C), 1301 (C–N), 1190 (C–O), 1087 (C–O–C), 742 (Ar–H, out-of-plane), 671 (C–Cl). ^{1}H NMR (400 MHz, DMSO-d_6) δ 10.05 (s, 1H, NH), 7.51–7.44 (m, 1H, Ar–H), 7.26 (t, J = 4.8 Hz, 2H, Ar–H), 7.08–7.01 (m, 1H, Ar–H), 4.50 (d, J = 8.0 Hz, 1H, CH), 3.40 (s, 3H, OCH_3), 3.01 (dd, J = 16.3, 8.0 Hz, 1H, CH_2), 2.42 (d, J = 16.3 Hz, 1H, CH_2), 2.29 (s, 3H, CH_3). ^{13}C NMR (101 MHz, DMSO-d_6) δ 169.57, 167.07, 150.43, 139.15, 132.78, 130.48, 129.11, 128.03, 127.76, 103.76, 51.59, 36.85, 35.30, 18.73.

3.1.2. Spectroscopic Characterization of Methyl 6-chloro-4-(substituted phenyl)-5-formyl-2-methyl-1,4-dihydropyridine-3-carboxylate Derivatives (M2, M5, M8, and M11)

3.1.2.1. Methyl 6-chloro-5-formyl-2-methyl-4-(4-nitrophenyl)-1,4-dihydropyridine-3-carboxylate (M2)

Light yellow; yield = 51.8%; Rf = 0.31; m.p. = 151 °C (Table 1). FT-IR (KBr, vmax, cm^{-1}): 3479 (N–H), 3061 (Ar–H), 2951, 2922, 2860 (C–H), 1697 (C=O, ester), 1649 (C=O, CHO), 1606, 1512 (C=C), 1558, 1344 (NO_2), 1294 (C–N), 1226, 1087 (C–O), 862, 692 (Ar–H). ^{1}H NMR (400 MHz, $CDCl_3$) δ 9.76 (s, 1H, CHO), 8.10 (d, J = 8.6 Hz, 2H, Ar–H), 7.46 (d, J = 8.6 Hz, 2H, Ar–H), 6.90 (s, 1H, NH), 5.22 (s, 1H, CH), 3.50 (s, 3H, OCH_3), 2.45 (s, 3H, CH_3). ^{13}C NMR (101 MHz, $CDCl_3$) δ 187.19, 166.50, 152.03, 146.73, 144.66, 142.07, 128.82, 123.69, 112.12, 105.41, 51.61, 38.74, 19.08.

3.1.2.2. Methyl 4-(4-bromophenyl)-6-chloro-5-formyl-2-methyl-1,4-dihydropyridine-3-carboxylate (M5)

Light yellow; yield = 59.3%; Rf = 0.35; m.p. = 141 °C (Table 1). FT-IR (KBr, vmax, cm^{-1}): 3464 (N–H), 3057 (Ar–H), 2951, 2920, 2848 (C–H), 1708 (C=O, ester), 1689 (C=O, CHO), 1600, 1539 (C=C), 1489 (C=C), 1296 (C–N), 1226, 1085 (C–O), 775, 731 (Ar–H), 630, 605 (C–Br). ^{1}H NMR (400 MHz, $CDCl_3$) δ 9.75 (s, 1H, CHO), 7.35 (d, J = 8.3 Hz, 2H, Ar–H), 7.15 (d, J = 8.3 Hz, 2H, Ar–H), 7.07 (s, 1H, NH), 5.09 (s, 1H, CH), 3.63 (s, 3H, OCH_3), 2.41 (s, 3H, CH_3). ^{13}C NMR (101 MHz, $CDCl_3$) δ 187.65, 167.00, 144.09, 142.17, 129.69, 120.83, 112.74, 106.13, 51.63, 38.14, 19.06.

3.1.2.3. Methyl 6-chloro-4-(4-chlorophenyl)-5-formyl-2-methyl-1,4-dihydropyridine-3-carboxylate (M8)

Light yellow; yield = 50%; Rf = 0.37; m.p. = 136 °C (Table 1). FT-IR (KBr, vmax, cm^{-1}): 3471 (N–H), 3062 (Ar–H), 2956, 2924, 2829 (C–H), 1710 (C=O, ester), 1689 (C=O, CHO), 1618, 1544 (C=C), 1487 (C=C), 1296 (C–N), 1226, 1085 (C–O), 804, 731 (Ar–H), 628, 455 (C–Cl). ^{1}H NMR (400 MHz, $CDCl_3$) δ 9.76 (s, 1H, CHO), 7.24–7.07 (m, 4H, Ar–H), 5.10 (s, 1H, CH), 3.63 (s, 3H, OCH_3), 2.40 (s, 3H, CH_3). ^{13}C NMR (101 MHz, $CDCl_3$) δ 187.61, 166.95, 144.14, 143.53, 142.23, 132.56, 129.20, 128.45, 112.68, 106.15,

51.51, 38.00, 18.90.

3.1.2.4. Methyl 6-chloro-4-(2-chlorophenyl)-5-formyl-2-methyl-1,4-dihydropyridine-3-carboxylate (M11)

Yellow; yield = 58%; Rf = 0.38; m.p. = 190 °C (Table 1). FT-IR (KBr, vmax, cm^{-1}): 3410 (N–H), 3057 (Ar–H), 2954, 2922, 2854 (C–H), 1707 (C=O, ester), 1633 (C=O, CHO), 1591, 1539 (C=C), 1487 (C=C), 1301 (C–N), 1230, 1087 (C–O), 831, 742 (Ar–H), 626, 453 (C–Cl). ^{1}H NMR (400 MHz, $CDCl_3$) δ 9.67 (s, 1H, CHO), 7.30 (d, J = 7.7 Hz, 2H, Ar–H), 7.20 (d, J = 6.5 Hz, 1H, Ar–H), 7.09 (t, J = 6.8 Hz, 1H, Ar–H), 7.02 (br s, 1H, NH), 5.39 (s, 1H, CH), 3.54 (s, 3H, OCH_3), 2.27 (s, 3H, CH_3). ^{13}C NMR (101 MHz, $CDCl_3$) δ 187.56, 167.06, 143.60, 142.41, 133.26, 131.73, 129.86, 128.02, 126.73, 112.32, 105.94, 51.23, 37.76, 18.83.

3.1.3. Spectroscopic Characterization of Methyl 6-chloro-4-(substituted phenyl)-2-methyl-5-(5-thioxo-1,2,4-triazolidin-3-yl)-1,4-dihydropyridine-3-carboxylate Derivatives (M3, M6, M9, and M12)

The TLC profile before purification showed multiple spots, whereas the chromatographic fractions showed improved separation and purity (Figure 1).

3.1.3.1. Methyl 6-chloro-2-methyl-4-(4-nitrophenyl)-5-(5-thioxo-1,2,4-triazolidin-3-yl)-1,4-dihydropyridine-3-carboxylate (M3)

Orange; yield = 50%; Rf = 0.20; m.p. = 226–228 °C (Table 1). FT-IR (KBr, vmax, cm^{-1}): 3545, 3419, 3317, 3236 (N–H, DHP and triazolidine rings), 3149 (Ar–H), 2947, 2918 (aliphatic C–H), 1639 (C=C), 1541 (NO_2, asym), 1342 (NO_2, sym), 1224 (C=S), 1103 (C–O–C). ^{1}H NMR (400 MHz, DMSO-d_6) δ 11.22 (s, 1H, NH), 9.93 (s, 1H, NH), 8.12 (s, 1H, NH), 8.08 (d, J = 8.7 Hz, 2H, Ar–H), 8.03 (s, 1H, triazolidine CH), 7.57 (d, J = 8.7 Hz, 2H, Ar–H), 7.35 (s, 1H, DHP–NH), 5.25 (s, 1H, DHP–CH), 3.54 (s, 3H, OCH_3), 2.28 (s, 3H, CH_3). ^{13}C NMR (101 MHz, DMSO-d_6) δ 177.48, 167.14, 154.65, 147.10, 146.41, 140.64, 131.75, 129.45, 123.64, 107.63, 101.07, 51.29, 40.63, 18.63. MS (m/z): $[M]^+$ = 409.

3.1.3.2. Methyl 4-(4-bromophenyl)-6-chloro-2-methyl-5-(5-thioxo-1,2,4-triazolidin-3-yl)-1,4-dihydropyridine-3-carboxylate (M6)

Orange; yield = 45%; Rf = 0.25; m.p. = 210–212 °C (Table 1). FT-IR (KBr, vmax, cm^{-1}): 3543, 3415, 3300 (N–H, DHP and triazolidine rings), 3037 (Ar–H), 2956, 2850 (aliphatic C–H), 1735 (C=O, ester), 1681 (C=C), 1371 (C–N), 1222 (C=S), 1039 (C–O–C), 617–561 (C–Br). ^{1}H NMR (400 MHz, DMSO-d_6) δ 11.23 (s, 1H, NH), 9.84 (s, 1H, NH), 8.12 (s, 1H, NH), 8.01 (s, 1H, triazolidine CH), 7.39 (d, J = 8.2 Hz, 2H, Ar–H), 7.25 (s, 1H, DHP–NH), 7.21 (d, J = 7.6 Hz, 2H, Ar–H), 5.07 (s, 1H, DHP–CH), 3.53 (s, 3H, OCH_3), 2.26 (s, 3H, CH_3). ^{13}C NMR (101 MHz, DMSO-d_6) δ 176.93, 166.91, 146.22, 146.07, 140.32, 131.48, 130.96, 130.80, 129.99, 119.32, 107.66, 101.20, 50.83, 40.66, 18.15. MS (m/z): $[M]^+$ = 443.

3.1.3.3. Methyl 6-chloro-4-(4-chlorophenyl)-2-methyl-5-(5-thioxo-1,2,4-triazolidin-3-yl)-1,4-dihydropyridine-3-carboxylate (M9)

Orange; yield = 62.3%; Rf = 0.22; m.p. = 208–210 °C (Table 1). FT-IR (KBr, vmax, cm^{-1}): 3425, 3145 (N–H, DHP and triazolidine rings), 3024 (Ar–H), 2974 (aliphatic C–H), 1751 (C=O, ester), 1662 (C=C), 1371 (C–N), 1222 (C=S), 1093 (C–O–C), 553–495 (C–Cl). ^{1}H NMR (400 MHz, DMSO-d_6) δ 11.23 (s, 1H, NH), 9.83 (s, 1H, NH), 8.11 (s, 1H, NH), 8.01 (s, 1H, triazolidine CH), 7.48 (s, 1H, DHP–NH), 7.26 (m, 4H, Ar–H), 5.08 (s, 1H, DHP–CH), 3.53 (s, 3H, OCH_3), 2.26 (s, 3H, CH_3). ^{13}C NMR (101 MHz, DMSO-d_6) δ 177.42, 167.35, 146.46, 146.21, 140.78, 131.20, 129.98, 128.32, 108.14, 107.59, 101.72, 51.23, 40.60, 18.57. MS (m/z): $[M]^+$ = 399.

3.1.3.4. Methyl 6-chloro-4-(2-chlorophenyl)-2-methyl-5-(5-thioxo-1,2,4-triazolidin-3-yl)-1,4-dihydropyridine-3-carboxylate (M12)

Orange; yield = 60%; Rf = 0.22; m.p. = 210–212 °C (Table 1). FT-IR (KBr, vmax, cm^{-1}): 3414, 3336, 3163 (N–H, DHP and triazolidine rings), 3030 (Ar–H), 2972 (aliphatic C–H), 1735 (C=O, ester), 1668 (C=C), 1371 (C–N), 1224 (C=S), 1035 (C–O–C), 547–420 (C–Cl). ^{1}H NMR (400 MHz, DMSO-d_6) δ 11.26 (s, 1H, NH), 9.94 (s, 1H, NH), 8.26 (s, 1H, NH), 8.07 (s, 1H, triazolidine CH), 7.36–7.19 (m, 4H, Ar–H), 7.16 (s, 1H, DHP–NH), 5.37 (s, 1H, DHP–CH), 3.51 (s, 3H, OCH_3), 2.24 (s, 3H, CH_3). ^{13}C NMR (101 MHz, DMSO-d_6) δ 177.29, 167.30, 146.14, 144.92, 141.54, 132.50, 131.36, 129.53, 128.61, 128.25, 107.82, 101.75, 51.06, 40.57, 18.43.

3.1.4. Molecular Docking Results

The docking protocol was evaluated by redocking the co-crystallized osimertinib into the active site of the L858R-mutant EGFR kinase domain. The highest-ranked redocked pose

reproduced the crystallographic orientation with a heavy-atom RMSD of 1.35 Å, which satisfied the predefined acceptance criterion of RMSD ≤ 2.0 Å. The corresponding GBVI/WSA dG score for osimertinib was −13.8 kcal/mol (Table 2), supporting use of the validated protocol for docking M3, M6, M9, and M12. This cutoff is consistent with the commonly applied criterion for successful reproduction of crystallographic ligand poses in docking-validation studies (Warren *et al*., 2006; Goullieux *et al*., 2023).

Among the synthesized compounds, M9 showed the most favorable predicted GBVI/WSA dG score (−15.9135 kcal/mol), followed by M6 (−14.6434 kcal/mol), M3 (−14.4948 kcal/mol), and M12 (−14.4427 kcal/mol). M9 formed a predicted hydrogen-bond donor interaction with Asp855, M6 an acceptor interaction with Thr790, M3 acceptor interactions with Lys745 and Gly796, and M12 an acceptor interaction with Lys745 (Table 2).

The comparatively high interaction-energy magnitude observed for M12 was verified from the original MOE output. This value reflects a specific ligand–residue interaction and does not indicate superior overall binding, as the total docking score depends on multiple energetic and geometric contributions.

The redocking result (RMSD = 1.35 Å) met the predefined validation criterion, and the reference-ligand score (GBVI/WSA dG = −13.8 kcal/mol) enabled comparison with the synthesized compounds. Nevertheless, docking scores are computational ranking estimates and should not be interpreted as experimentally measured binding energies.

3.2. Discussion

3.2.1. Discussion of Step 1 (Hantzsch Reaction)

The Hantzsch-type multicomponent reaction afforded the expected 1,4,5,6-tetrahydropyridine derivatives M1, M4, M7, and M10 in moderate yields. The observed N–H, ester C=O, and lactam C=O bands, together with the aromatic, methine, methylene, methoxy, methyl, and N–H resonances, are consistent with Hantzsch-derived dihydropyridine systems reported previously (Vijesh *et al*., 2011; Hussein and Al-Mathkuri, 2025). The nonequivalent CH_2 protons showed the expected diastereotopic splitting pattern, and the ^{13}C NMR and DEPT-135 spectra supported the assigned carbon environments. Because no mechanistic or purification data specifically explain the lower yield of M7, no causal explanation is proposed.

3.2.2. Discussion of Step 2 (Vilsmeier–Haack Formylation)

Vilsmeier–Haack formylation converted the tetrahydropyridine intermediates into the corresponding 5-formyl-1,4-dihydropyridine derivatives M2, M5, M8, and M11, in agreement with the transformation reported for related substrates (Armas *et al*., 2000). The disappearance of the lactam carbonyl and CH_2 features, together with aldehydic ^1H signals at δ 9.67–9.76 ppm and ^{13}C signals near δ 187 ppm, supports successful formylation. The downfield aldehyde resonances are also consistent with established carbonyl-anisotropy effects in aromatic aldehydes and ketones (Abraham, Mobli, and Smith, 2003).

3.2.3. Discussion of Step 3 (Cyclization to Triazolidine Derivatives)

Reaction of the formylated intermediates with thiosemicarbazide afforded the proposed 1,2,4-triazolidine-3-thione derivatives M3, M6, M9, and M12. Loss of the aldehyde carbonyl and aldehydic proton signals, together with the appearance of a C=S band near 1222 cm^{-1} and additional NH and ring-CH resonances, supports cyclization. Comparable thiosemicarbazone-to-triazolidine-3-thione transformations have been reported by Gričar *et al.* (2025), Patil *et al.* (2019), and Ramesh and Lalitha (2016). The downfield NH resonances in DMSO-d_6 are compatible with solvent and hydrogen-bonding effects described for amide-type protons (Abraham, Griffiths, and Perez, 2014).

The combined FT-IR, ^1H NMR, ^{13}C NMR, DEPT-135, and mass-spectral data support the proposed structures; however, two-dimensional NMR spectroscopy or single-crystal X-ray diffraction would provide more definitive structural and stereochemical confirmation. This limitation should be considered when interpreting the assignments.

3.2.4. Substituent Effects and Molecular Docking Analysis

The final compounds showed a narrow range of predicted docking scores, with M9 ranked highest, followed by M6, M3, and M12. The more favorable score of the para-chloro derivative M9 relative to the ortho-chloro derivative M12 is consistent with a possible positional effect on ligand accommodation, but the four-compound series is too small to establish a definitive structure–activity relationship. Similar EGFR-focused docking studies of dihydropyridine derivatives have also emphasized the influence of aryl substitution on predicted binding behavior

(Mansour *et al.*, 2022; Faizan *et al.*, 2024).

The predicted interaction profiles involved residues within the EGFR ATP-binding region. M3 showed acceptor contacts with Lys745 and Gly796, M6 with Thr790, M9 a donor contact with Asp855, and M12 an acceptor contact with Lys745. These contacts provide a structural basis for comparing the four poses, but the GBVI/WSA dG score should be interpreted as a ranking metric rather than a direct measure of binding affinity.

M9 combined the most negative docking score with a predicted interaction involving Asp855, whereas M6, M3, and M12 showed slightly less favorable scores and different contact patterns. This ranking is broadly consistent with prior computational work in which dihydropyridine derivatives occupied the EGFR ATP-binding pocket and interacted with catalytically relevant residues (Mansour et al., 2022). Relative to the validated osimertinib reference score of −13.8 kcal/mol (RMSD = 1.35 Å), all four synthesized compounds produced more negative GBVI/WSA dG scores under the applied protocol, with M9 showing the largest numerical difference. This comparison remains computational and does not establish superior experimental affinity or potency.

The substituent-dependent differences are therefore best viewed as preliminary qualitative observations. Additional analogs, independent docking validation, molecular dynamics simulations, and binding free-energy calculations would be needed to test whether the observed ranking is robust. Broader EGFR inhibitor programs likewise combine structural optimization with biochemical, cellular, and in vivo validation rather than relying on docking scores alone (Wang *et al.*, 2022).

Overall, the docking findings provide a hypothesis for subsequent experimental work but do not demonstrate EGFR inhibition or anticancer activity. Validation should include biochemical EGFR kinase assays, cell-based cytotoxicity testing, and selectivity assessment in non-malignant cells.

4. CONCLUSIONS

A new series of 1,4-dihydropyridine–1,2,4-triazolidine-3-thione hybrid derivatives was synthesized through Hantzsch-type condensation, Vilsmeier–Haack formylation, and cyclization with thiosemicarbazide. FT-IR, ^{1}H-NMR, ^{13}C-NMR, DEPT-135, and mass-spectrometric data supported the proposed structures.

Molecular docking against the EGFR tyrosine kinase domain ranked M9 highest under the applied computational conditions (GBVI/WSA dG = −15.9135 kcal/mol), followed by M6, M3, and M12. The compounds showed distinct predicted contacts within the EGFR binding pocket.

These computational results are preliminary and do not confirm EGFR inhibition or anticancer activity. The docking protocol was validated by redocking osimertinib (heavy-atom RMSD = 1.35 Å; GBVI/WSA dG = −13.8 kcal/mol). The synthesized compounds, particularly M9, warrant further evaluation through in vitro EGFR kinase assays, cytotoxicity testing, selectivity assessment, and independent computational validation.

5. DECLARATIONS

5.1. Study Limitations

No *in vitro* or *in vivo* biological evaluation was performed; therefore, the docking results represent preliminary computational predictions only. EGFR kinase inhibition, cytotoxicity, cellular selectivity, and mechanism-based biological assays are required to validate the proposed activity.

Structural assignment of the final triazolidine-3-thione derivatives relied on FT-IR, ^{1}H-NMR, ^{13}C-NMR, DEPT-135, and mass spectrometry. Two-dimensional NMR spectroscopy or single-crystal X-ray diffraction would provide more definitive structural and stereochemical confirmation.

The docking analysis used a single software platform, one receptor structure, and a limited compound series. Independent docking, molecular-dynamics simulations, and binding free-energy calculations would strengthen the computational conclusions. Moderate yields and the use of column chromatography for several compounds may also limit scalability.

Although the docking protocol met the predefined redocking criterion using osimertinib (RMSD = 1.35 Å), the analysis was limited to one software platform, one receptor structure, and a small compound series. Independent docking, molecular-dynamics simulations, binding free-energy calculations, and experimental EGFR-inhibition assays are therefore required to test the

robustness and biological relevance of the predicted ranking.

5.2. Acknowledgments

The authors would like to thank the Department of Chemistry, College of Science, University of Misan, for providing laboratory facilities.

5.3. Funding

The authors funded this research.

5.4. Conflicts of Interest

The authors declare that they have no competing interests.

5.5. Data Availability

The data supporting the findings of this study are available from the corresponding author upon reasonable request.

5.6. Author Contributions

Maryam Sabri Hashim: CD, DC, DAI, MW, FA.

Tahseen Saddam Fandi Al-Mathkuri: CD, DAI, CR, FA.

Code	English	Português
CD	Conception and Design	Concepção e Design
DC	Data Collection	Coleta de Dados
DAI	Data Analysis and Interpretation	Análise e Interpretação de Dados
MW	Manuscript Writing	Escrita do Manuscrito
CR	Critical Review	Revisão Crítica
FA	Final Approval	Aprovação Final

5.7. AI and Computational Tools Declaration

The authors used Molecular Operating Environment (MOE, version 2014; Chemical Computing Group Inc., Montreal, Canada) for molecular docking and ligand–protein interaction analysis. QuillBot was used only for language editing and readability improvement. The authors are responsible for all scientific content, data analysis, and interpretation.

5.8. Research Integrity Declaration

The authors confirm that this manuscript is original, has not been published previously, and is not under consideration for publication elsewhere.

5.9. Originality and Plagiarism Statement

This manuscript is original, has not been published previously, and is not under consideration for publication elsewhere. The manuscript was screened for textual similarity, and the similarity index was 9%, which is within the acceptable limit. All sources and previously published materials have been appropriately cited and acknowledged.

5.10. Open Access License

6. STUDIES INVOLVING HUMAN AND ANIMAL SUBJECTS

6.1. Ethics Committee Approval

Not applicable.

6.2. Informed Consent

Not applicable.

7. REFERENCES

1. Abdel-Hafez, S. H. (2008). Selenium-containing heterocycles: Synthesis, anti-inflammatory, analgesic, and antimicrobial activities of some new 4-cyanopyridazine-

3(2H)-selenone derivatives. European Journal of Medicinal Chemistry, 43(9), 1971–1977. https://doi.org/10.1016/j.ejmech.2007.12.006

2. Abraham, R. J., Griffiths, L., and Perez, M. (2014). ^{1}H NMR spectra part 31: ^{1}H chemical shifts of amides in DMSO solvent. Magnetic Resonance in Chemistry, 52(7), 395–408. https://doi.org/10.1002/mrc.4079
3. Abraham, R. J., Mobli, M., and Smith, R. J. (2003). ^{1}H chemical shifts in NMR: Part 19. Carbonyl anisotropies and steric effects in aromatic aldehydes and ketones. Magnetic Resonance in Chemistry, 41(1), 26–36. https://doi.org/10.1002/mrc.1125
4. Ali, A. S., and Al-Mathkuri, T. S. F. (2023). Synthesis and study of the effect of new pyrazoles and oxadiazoles linked to the 1,4-dihydropyridine ring on breast cancer. Journal of Chemical Health Risks, 13(4), 701–719. https://doi.org/10.22034/jchr.2023.1996251.1817
5. Armas, N., Blaton, N. M., Peeters, O. M., De Ranter, C. J., Su, M., Ochoa, E., and Verdecia, Y. (2000). Synthesis, crystal structure, and molecular modeling of methyl 6-chloro-4-(2-chlorophenyl)-5-formyl-2-methyl-1,4-dihydropyridine-3-carboxylate. Journal of Chemical Crystallography, 30(4), 235–241. https://doi.org/10.1023/A:1009590405705
6. Burley, S. K., Berman, H. M., Bhikadiya, C., Bi, C., Chen, L., Di Costanzo, L., Christie, C., Dalenberg, K., Duarte, J. M., Dutta, S., Feng, Z., Ghosh, S., Goodsell, D. S., Green, R. K., Guranovic, V., Guzenko, D., Hudson, B. P., Kalro, T., Liang, Y., Lowe, R., Namkoong, H., Peisach, E., Periskova, I., Prlić, A., Randle, C., Rose, A., Rose, P., Sala, R., Sekharan, M., Shao, C., Tan, L., Tao, Y.-P., Valasatava, Y., Voigt, M., Westbrook, J., Woo, J., Yang, H., Young, J., Zhuravleva, M., and Zardecki, C. (2019). RCSB Protein Data Bank: Biological macromolecular structures enabling research and education in fundamental biology, biomedicine, biotechnology and energy. Nucleic Acids Research, 47(D1), D464–D474. https://doi.org/10.1093/nar/gky1004
7. Chalán-Gualán, S., Castro, V., Oropeza, R., Suárez, M., Albericio, F., and Rodríguez, H. (2022). 3,4-Dihydro-2(1H)-pyridones as building blocks of synthetic relevance. Molecules, 27(16), 5070. https://doi.org/10.3390/molecules27165070
8. Comins, D. L., and Ma, D. (2016). Editorial for the special issue on heterocycles. Journal of Organic Chemistry, 81(21), 10107–10108. https://doi.org/10.1021/acs.joc.6b02488
9. Cross, D. A. E., Ashton, S. E., Ghiorghiu, S., Eberlein, C., Nebhan, C. A., Spitzler, P. J., Orme, J. P., Finlay, M. R. V., Ward, R. A., Mellor, M. J., Hughes, G., Rahi, A., Jacobs, V. N., Brewer, M. R., Ichihara, E., Sun, J., Jin, H., Ballard, P., Al-Kadhimi, K., Rowlinson, R., Klinowska, T., Richmond, G. H. P., Cantarini, M., Kim, D.-W., Ranson, M. R., and Pao, W. (2014). AZD9291, an irreversible EGFR TKI, overcomes T790M-mediated resistance to EGFR inhibitors in lung cancer. Cancer Discovery, 4(9), 1046–1061. https://doi.org/10.1158/2159-8290.CD-14-0337
10. Faizan, S., Talath, S., Wali, A. F., Hani, U., Haider, N., Mandal, S. P., and Kumar, B. R. P. (2024). Anticancer potential of novel symmetrical and asymmetrical dihydropyridines against breast cancer via EGFR inhibition. RSC Advances, 14, 11368–11387. https://doi.org/10.1039/D4RA01424C
11. Goullieux, M., Zoete, V., and Röhrig, U. F. (2023). Two-step covalent docking with Attracting Cavities. Journal of Chemical Information and Modeling, 63(24), 7847–7859. https://doi.org/10.1021/acs.jcim.3c01055
12. Gričar, S., Počkaj, M., Marolt, G., Bogojević, S. Š., Novinec, M., and Kljun, J. (2025). Spontaneous cyclization of 2-methylthiosemicarbazones yields new 1,2,4-triazolidine-3-thiones useful as building blocks for drug design. ChemistrySelect, 10, e202404001. https://doi.org/10.1002/slct.202404001
13. Heravi, M. M. (2020). Prescribed drugs containing nitrogen heterocycles: An overview. RSC Advances, 10, 44247–44311. https://doi.org/10.1039/D0RA09198G
14. Hussein, S. K., and Al-Mathkuri, T. S. F. (2025). Eco-friendly iodine-catalyzed synthesis and spectroscopic characterization of novel 1,4-dihydropyridine derivatives. New Materials, Compounds and Applications, 9(3), 611–628. https://doi.org/10.62476/nmca.93611
15. Irfan, A., Hussain, T., Nasim, I., Mojzych, M., and Zaki, M. E. A. (2025). Recent advances in nitrogenous heterocycle-based drugs and EGFR inhibitors for precision oncology (2020–2024): A review. Journal of Saudi Chemical Society, 29, 39. https://doi.org/10.1007/s44442-025-00040-y
16. Kabir, E., and Uzzaman, M. (2022). A review

on biological and medicinal impact of heterocyclic compounds. Results in Chemistry, 4, 100606. https://doi.org/10.1016/j.rechem.2022.100606
17. Lago, A. F. S., de Benedicto, D. F. C., da Silva, L., and Thomasi, S. S. (2023). 1,4-Dihydropyridine derivatives: An overview of synthesis conditions and biological tests. Current Organic Chemistry, 27(18), 1567–1610. https://doi.org/10.2174/0113852728264228231013074432
18. Mansour, B., Bayoumi, W. A., El-Sayed, M. A., Abouzeid, L. A., and Massoud, M. A. M. (2022). In vitro cytotoxicity and docking study of novel symmetric and asymmetric dihydropyridines and pyridines as EGFR tyrosine kinase inhibitors. Chemical Biology and Drug Design, 100(1), 121–135. https://doi.org/10.1111/cbdd.14058
19. Patil, P. J., Salunke, G. D., Deshmukh, M. B., Hangirgekar, S. P., Chandam, D. R., and Sankpal, S. A. (2019). Thiamine hydrochloride-catalyzed synthesis of 1,2,4-triazolidine-3-thiones in aqueous medium. ChemistrySelect, 4(45), 13071–13078. https://doi.org/10.1002/slct.201903646
20. Ramesh, R., and Lalitha, A. (2016). Facile and green-chemistry access to 5-aryl-1,2,4-triazolidine-3-thiones in aqueous medium. ChemistrySelect, 1(9), 2085–2089. https://doi.org/10.1002/slct.201600348
21. Soni, A., Sharma, M., and Singh, R. K. (2025). A decade of catalytic progress in 1,4-dihydropyridines (1,4-DHPs) synthesis (2016–2024). Current Organic Synthesis, 22(6), 703–720. https://doi.org/10.2174/0115701794374153250307065611
22. Vijesh, A. M., Isloor, A. M., Peethambar, S. K., Shivananda, K. N., Arulmoli, T., and Isloor, N. A. (2011). Hantzsch reaction: Synthesis and characterization of new 1,4-dihydropyridine derivatives. European Journal of Medicinal Chemistry, 46(11), 5591–5597. https://doi.org/10.1016/j.ejmech.2011.09.026
23. Vitaku, E., Smith, D. T., and Njardarson, J. T. (2014). Analysis of the structural diversity, substitution patterns, and frequency of nitrogen heterocycles among U.S. FDA-approved pharmaceuticals. Journal of Medicinal Chemistry, 57(24), 10257–10274. https://doi.org/10.1021/jm501100b
24. Warren, G. L., Andrews, C. W., Capelli, A.-M., Clarke, B., LaLonde, J., Lambert, M. H., Lindvall, M., Nevins, N., Semus, S. F., Senger, S., Tedesco, G., Wall, I. D., Woolven, J. M., Peishoff, C. E., and Head, M. S. (2006). A critical assessment of docking programs and scoring functions. Journal of Medicinal Chemistry, 49(20), 5912–5931. https://doi.org/10.1021/jm050362n
25. Wang, C., Wang, X., Huang, Z., Wang, T., Nie, Y., Yang, S., Xiang, R., and Fan, Y. (2022). Discovery and structural optimization of potent epidermal growth factor receptor (EGFR) inhibitors against the L858R/T790M/C797S resistance mutation for lung cancer treatment. European Journal of Medicinal Chemistry, 237, 114381. https://doi.org/10.1016/j.ejmech.2022.114381
26. Zhao, S., Zhang, X., Wei, P., Su, X., Zhao, L., Wu, M., and Hao, C. (2017). Design, synthesis, and evaluation of aromatic heterocyclic derivatives as antifungal agents. European Journal of Medicinal Chemistry, 137, 96–107. https://doi.org/10.1016/j.ejmech.2017.05.043

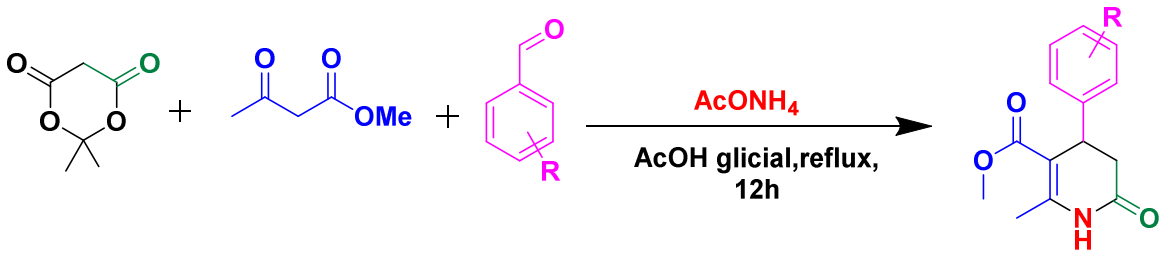

R=4-NO_2 , 4-Br , 4-Cl , 2-Cl
M1 M4 M7 M10

Equation 1. *Synthesis of 1,4,5,6-tetrahydropyridine-3-carboxylate derivatives.*

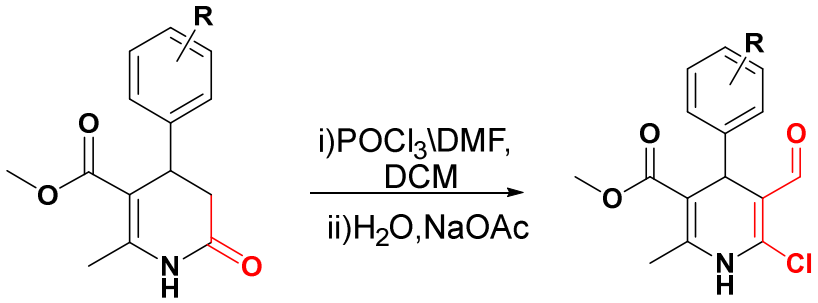

R= 4-NO_2 , 4-Br ,4-Cl ,2-Cl
M2 M5 M8 M11

Equation 2. *Synthesis of 5-formyl-1,4-dihydropyridine derivatives.*

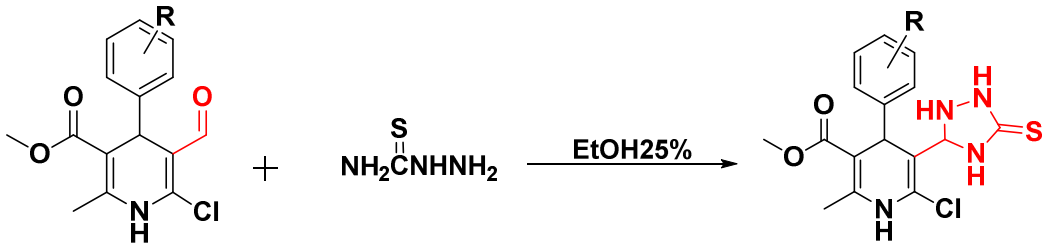

R= 4-NO_2 , 4-Br ,4-Cl ,2-Cl
M3 M6 M9 M12

Equation 3. *Synthesis of 1,4-dihydropyridine–1,2,4-triazolidine-3-thione derivatives.*

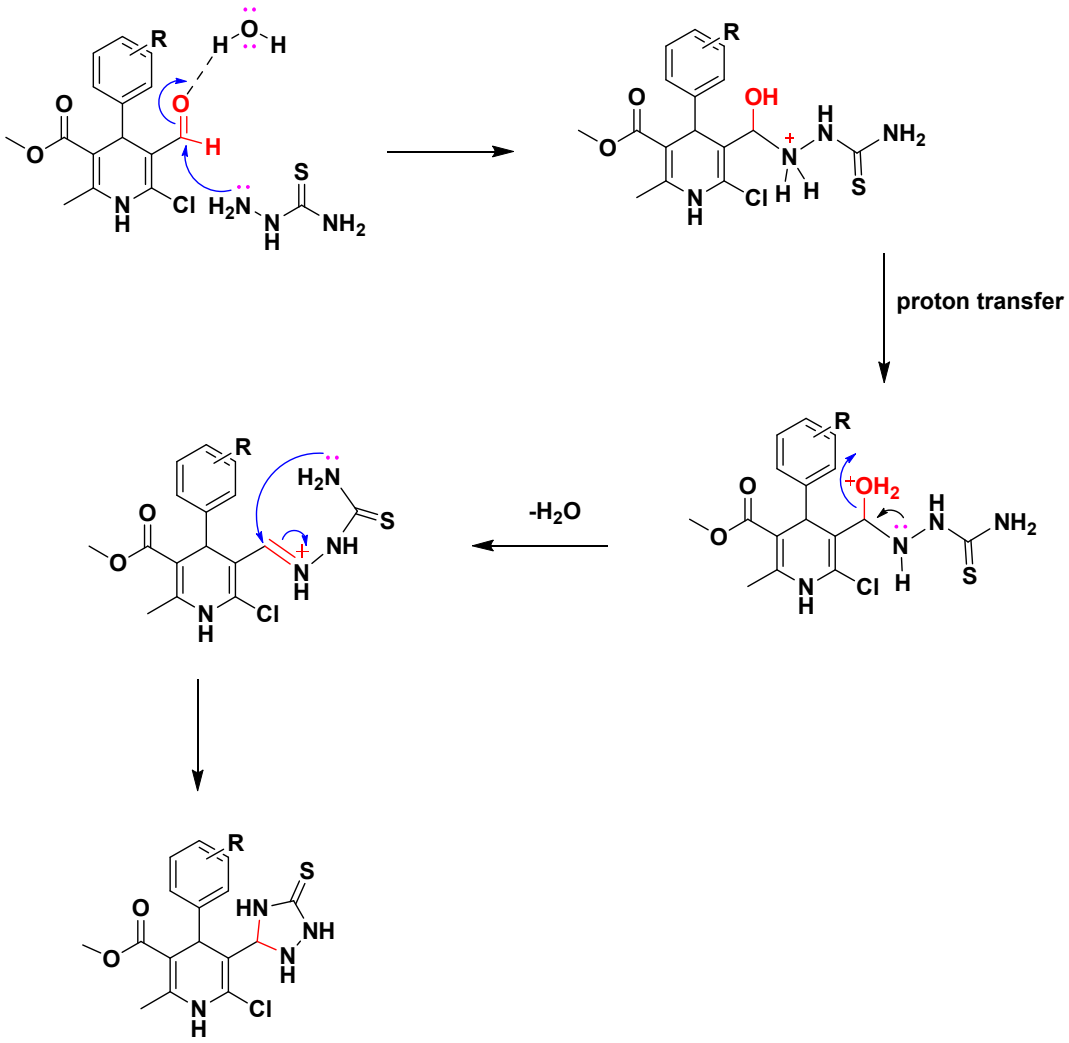

Scheme 1. *Proposed mechanism for cyclization of the formylated intermediates with thiosemicarbazide to afford 1,2,4-triazolidine-3-thione derivatives.*

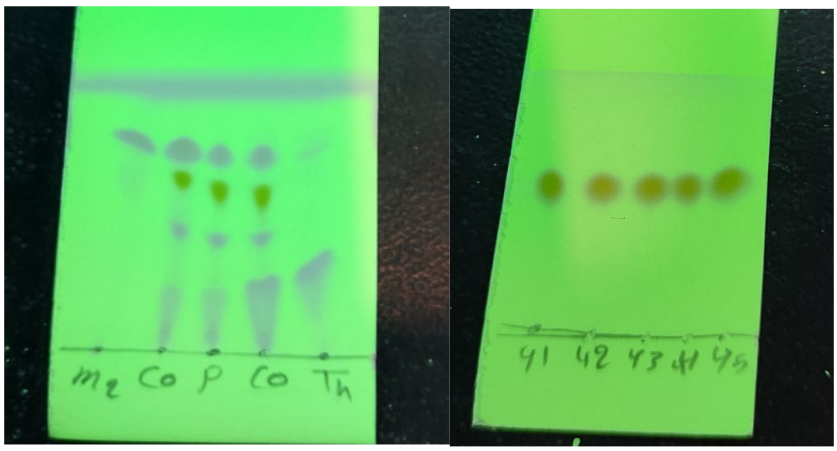

(a) (b)

Figure 1. *TLC analysis of compound M3 during step 3: (a) reaction-mixture profile before purification; (b) column-chromatography fractions obtained using ethyl acetate/petroleum ether (1:3, v/v).*

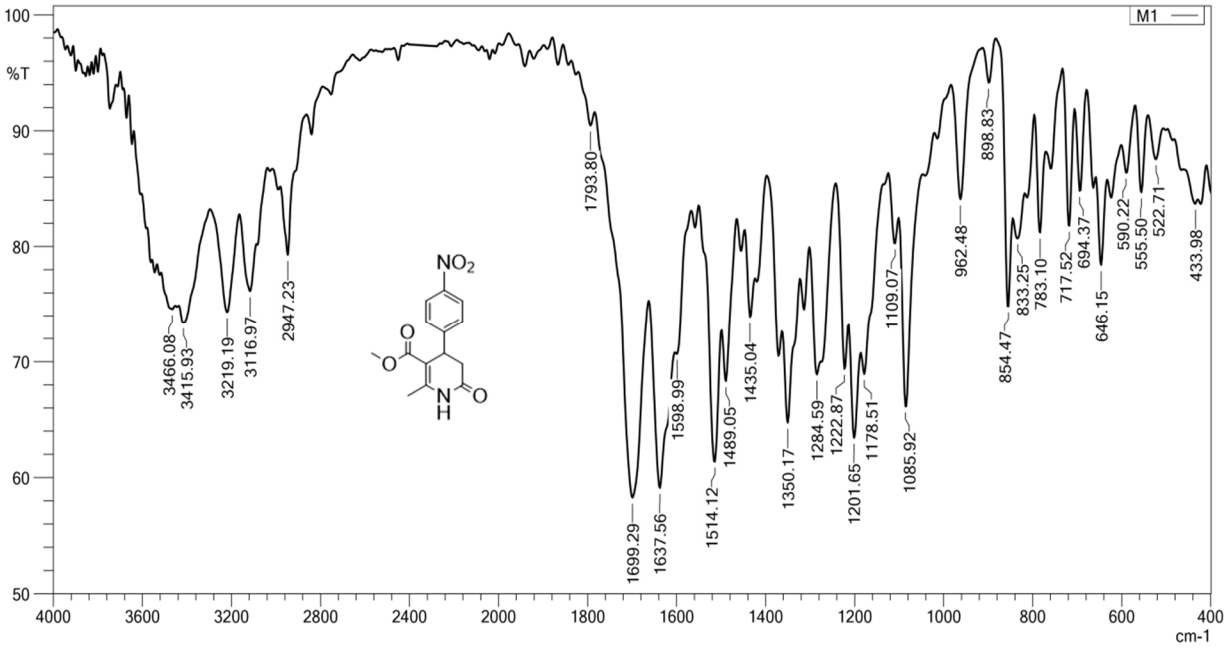

Figure 2. *FT-IR spectrum of compound M1 (KBr, 4000–400 cm⁻¹).*

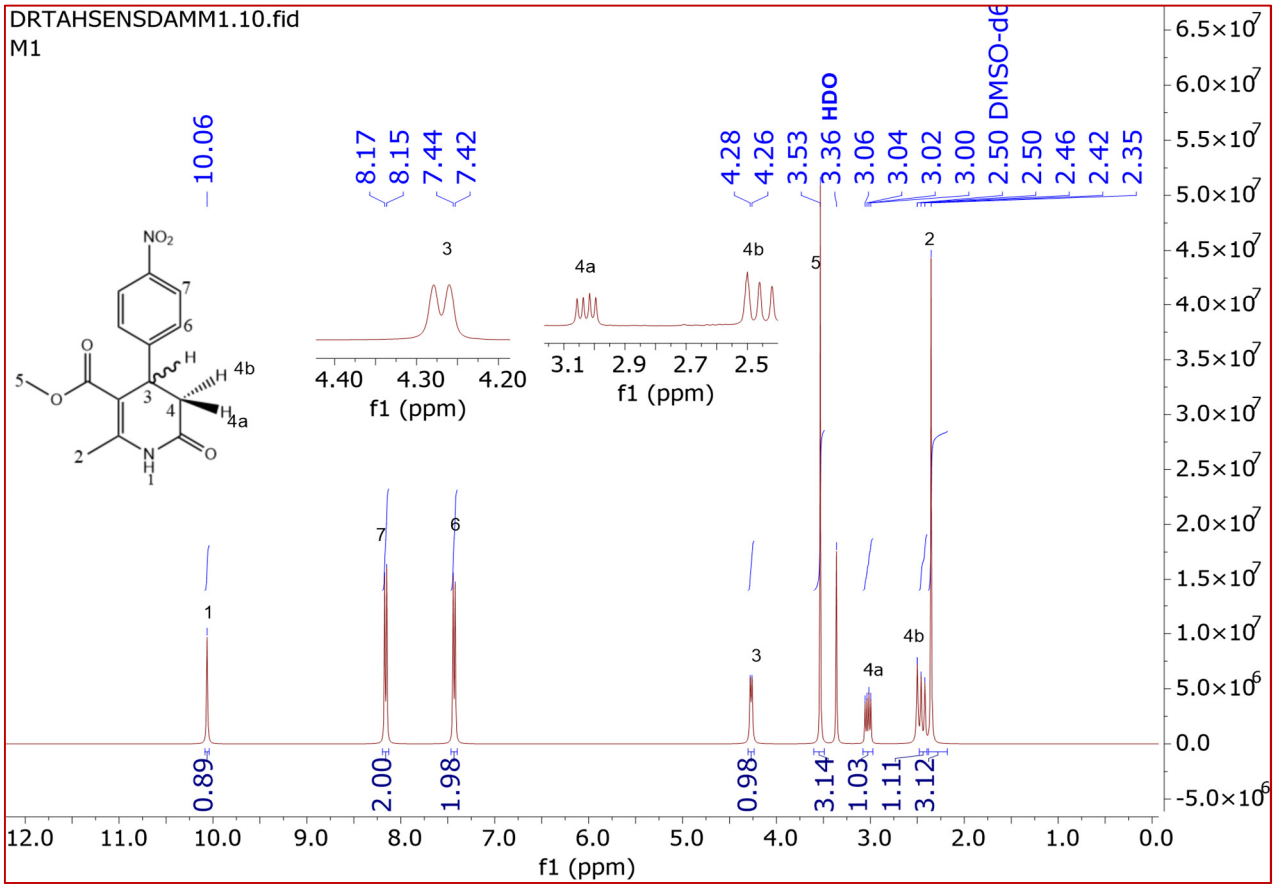

Figure 3. *¹H-NMR spectrum of compound M1 (400 MHz, DMSO-d_6).*

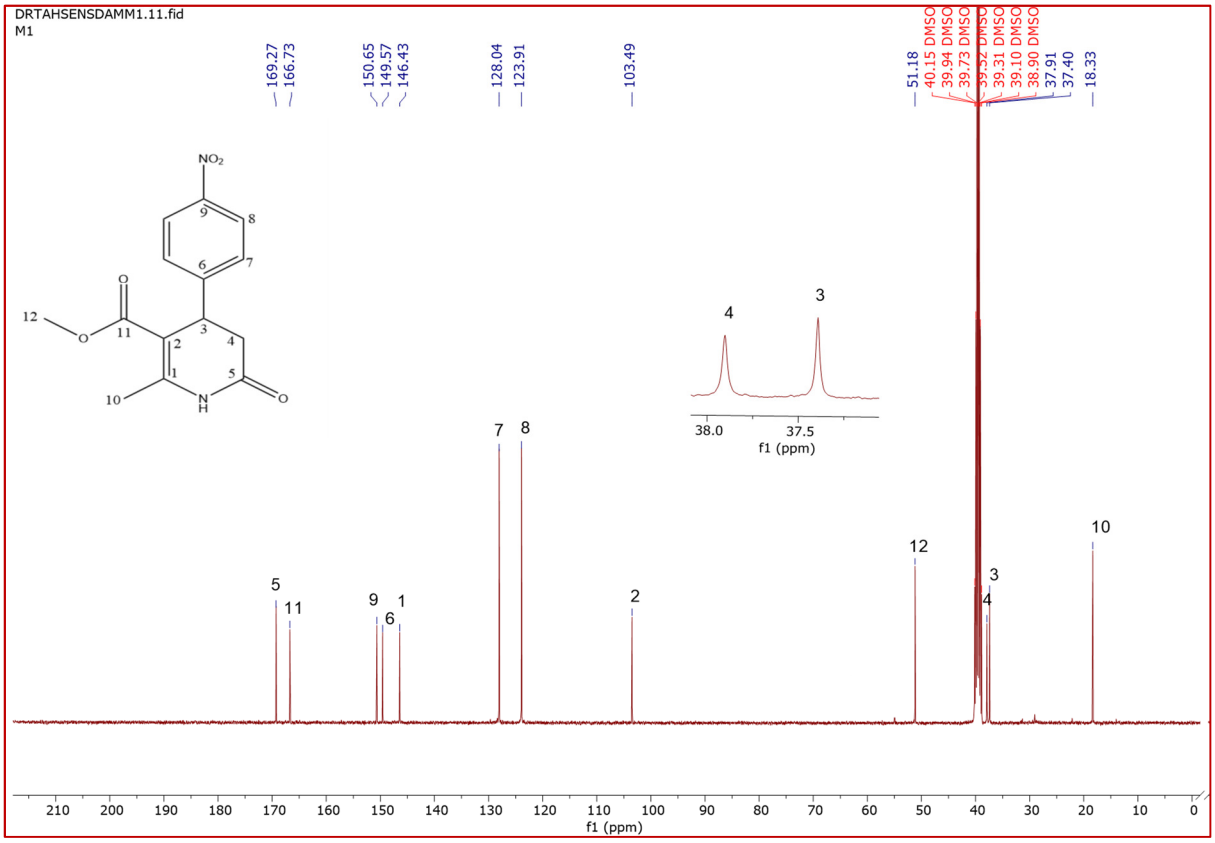

Figure 4. *^{13}C-NMR spectrum of compound M1 (101 MHz, DMSO-d_6).*

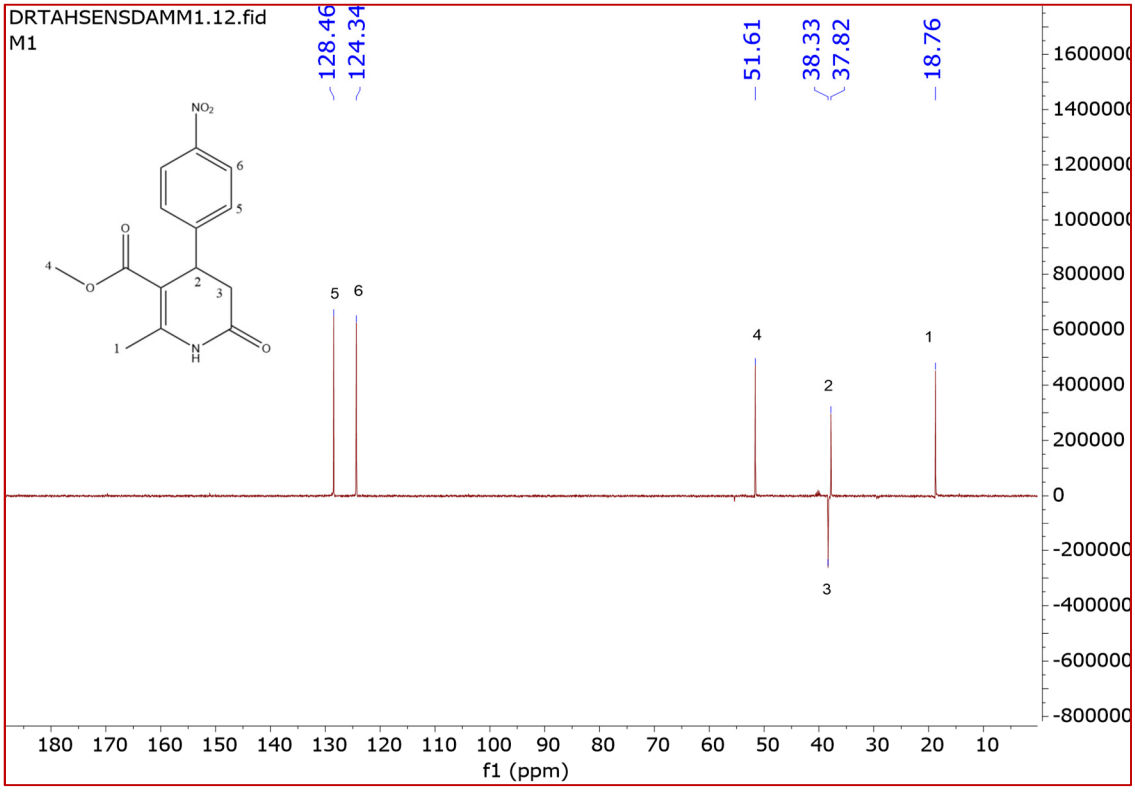

Figure 5. *DEPT-135 spectrum of compound M1.*

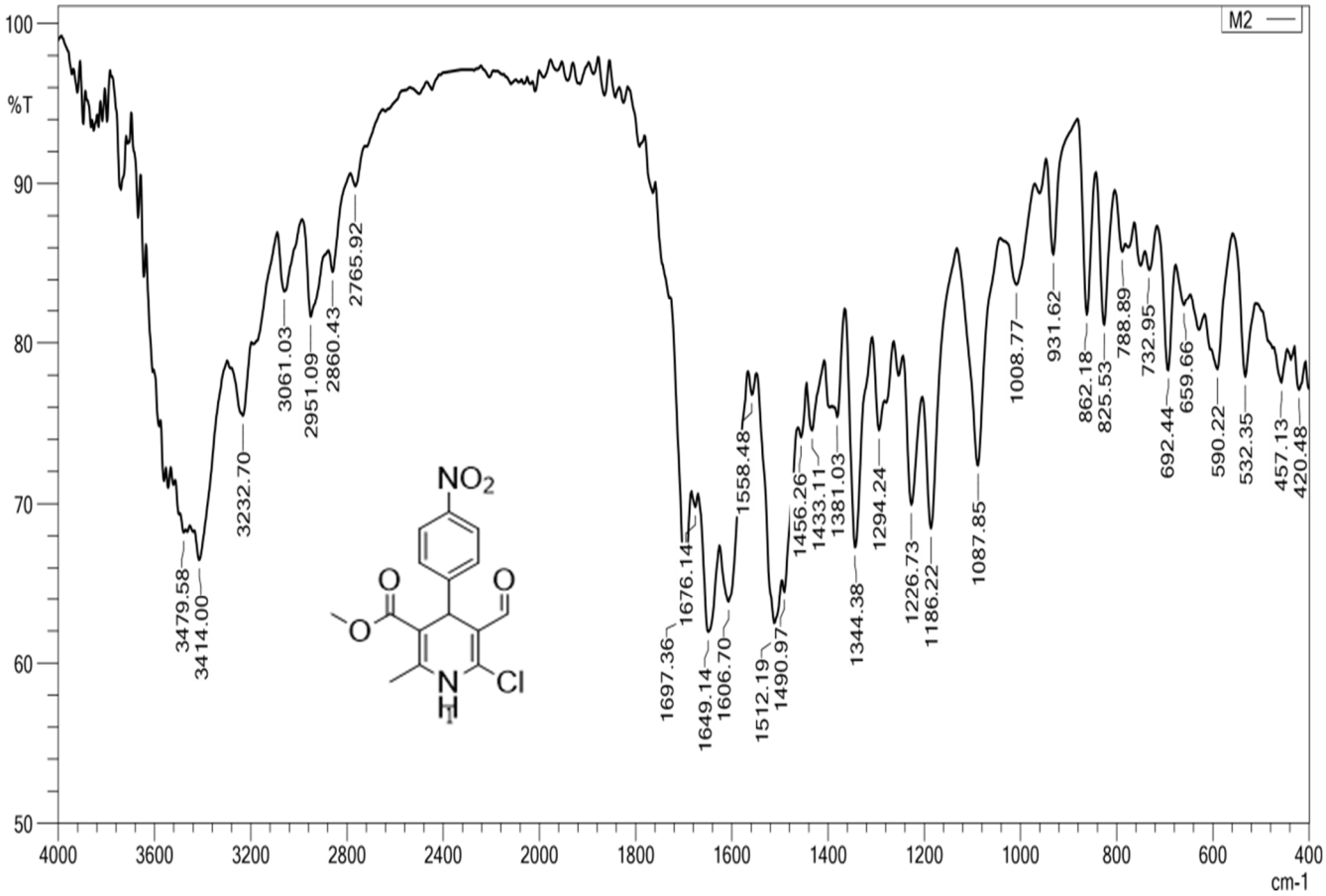

***Figure 6**. FT-IR spectrum of compound M2 (KBr, 4000–400 cm⁻¹).*

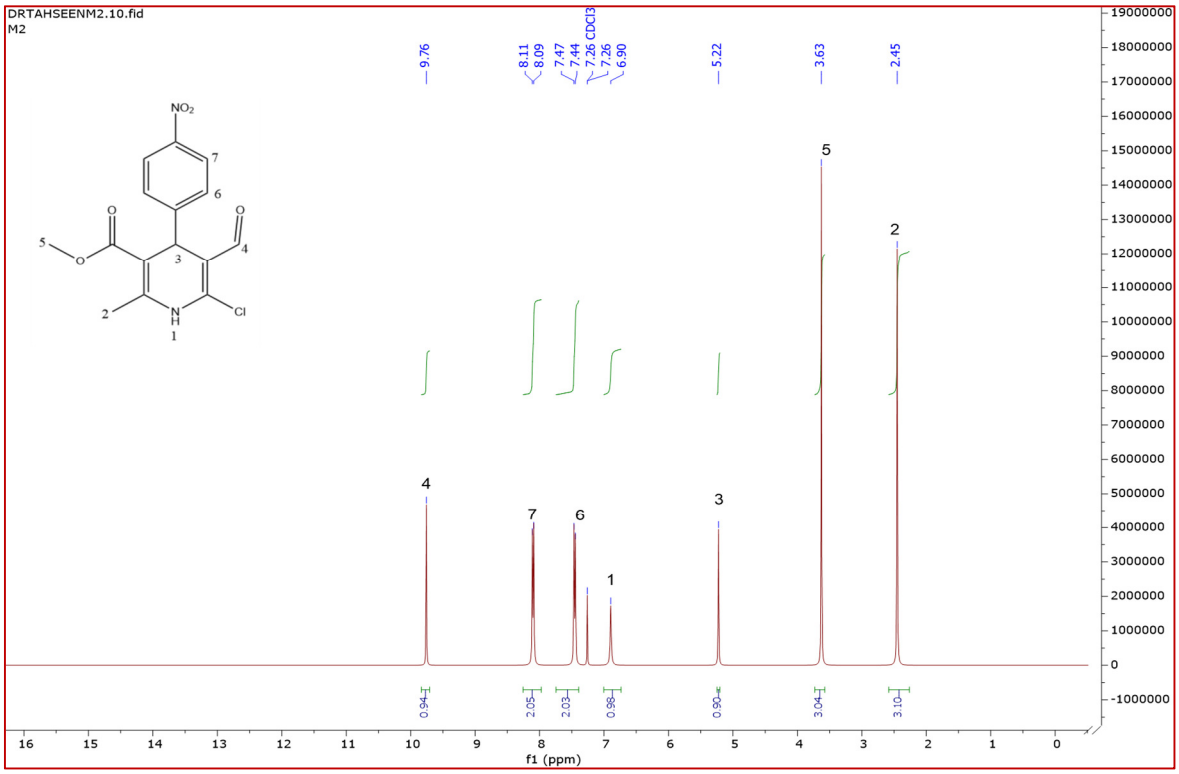

***Figure 7**. ¹H-NMR spectrum of compound M2 (400 MHz, $CDCl_3$).*

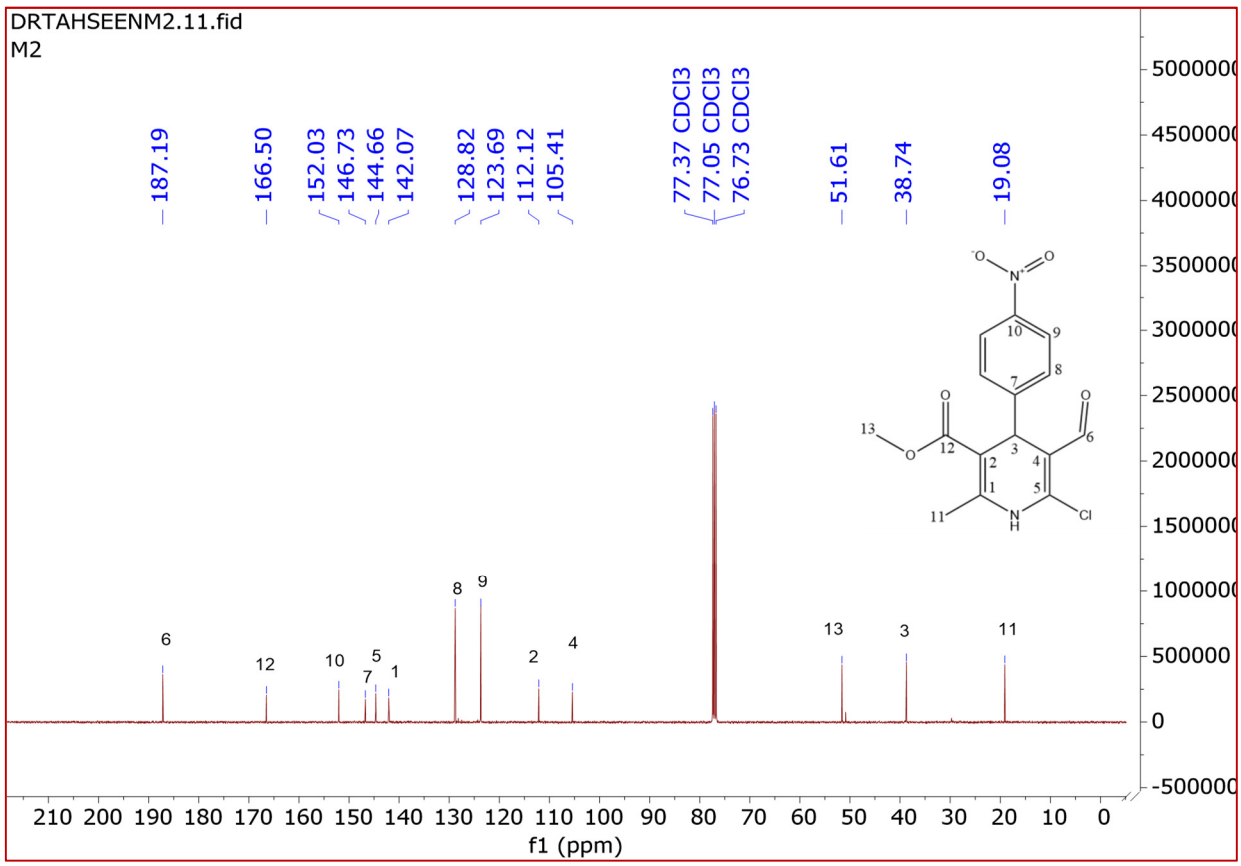

Figure 8. *^{13}C-NMR spectrum of compound M2 (101 MHz, $CDCl_3$).*

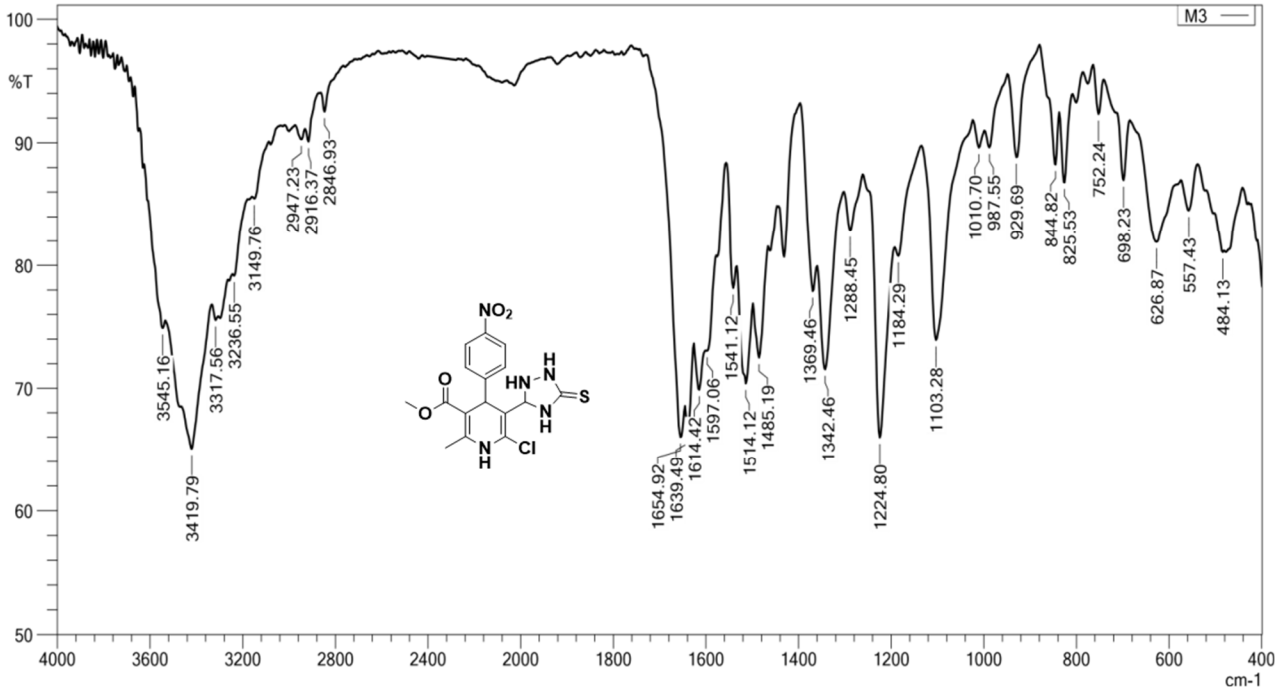

Figure 9. *FT-IR spectrum of compound M3 (KBr, 4000–400 cm^{-1}).*

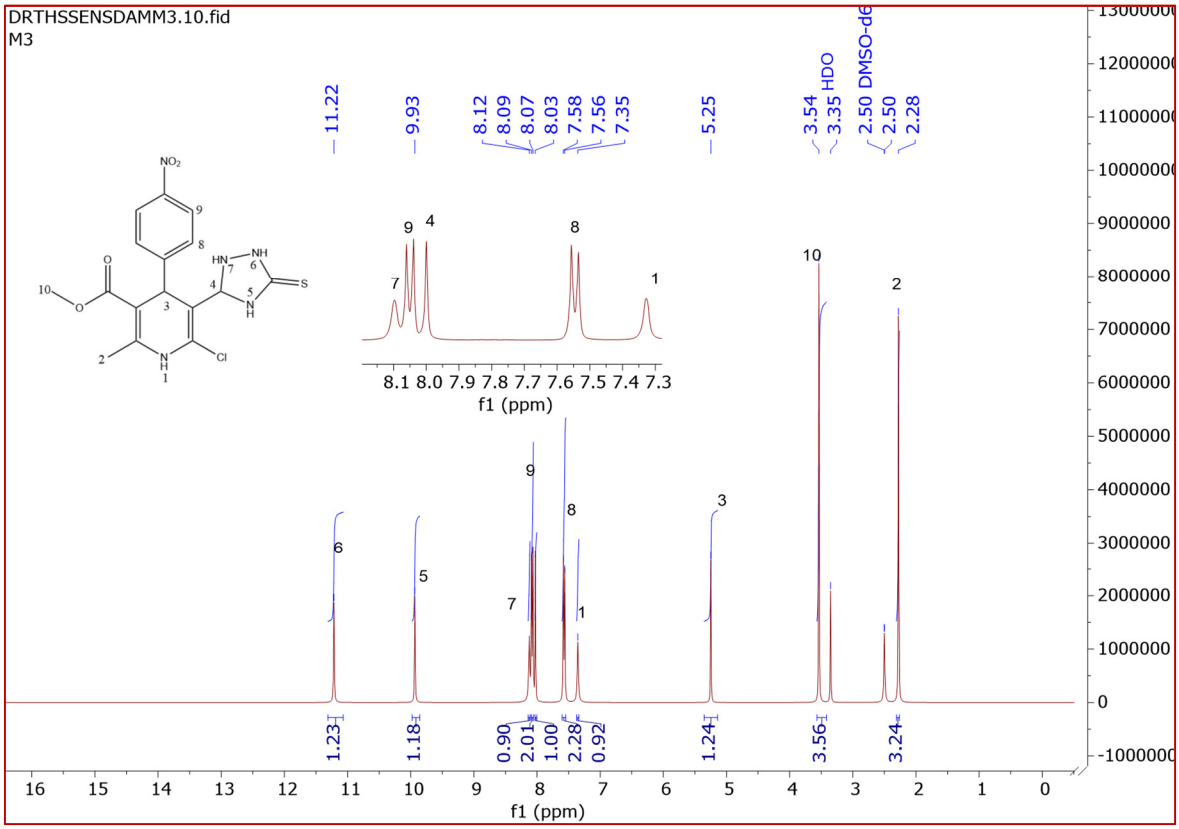

Figure 10. *¹H-NMR spectrum of compound M3 (400 MHz, DMSO-d_6).*

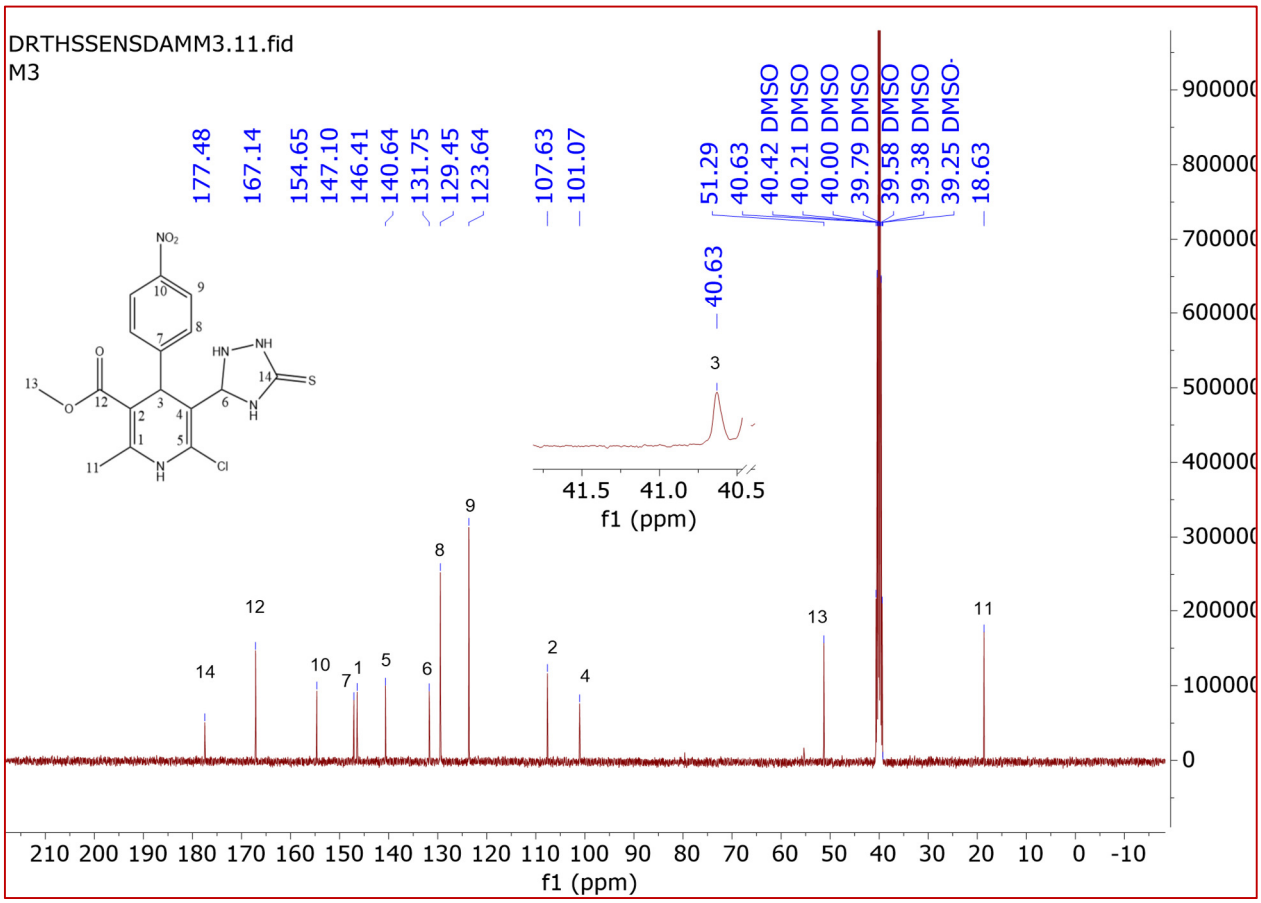

Figure 11*. ¹³C-NMR spectrum of compound M3 (101 MHz, DMSO-d_6).*

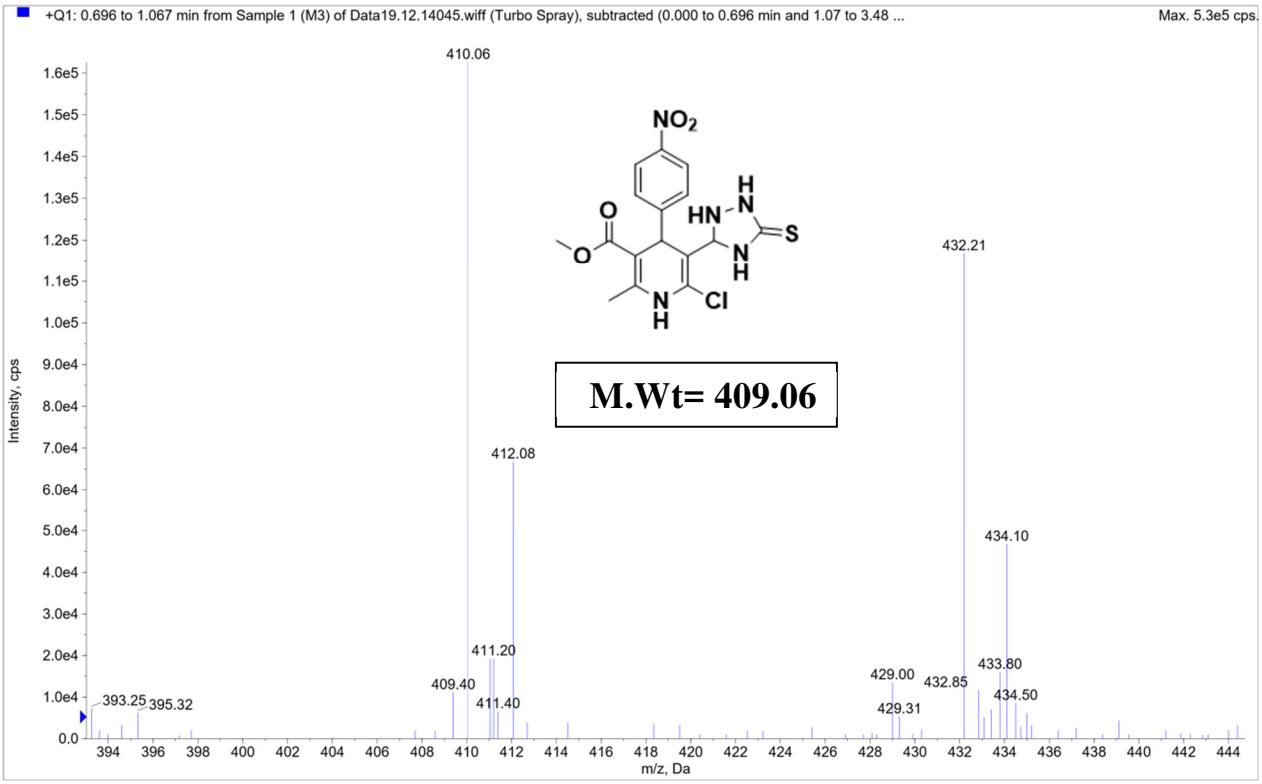

***Figure 12**. ESI mass spectrum of compound M3.*

***Table 1**. Physical characteristics, reaction yields, molecular formulae, and structures of the synthesized compounds M1–M12.*

Compound	Structural formula	Molecular formula	Color	m.p. (°C)	Yield (%)
M1	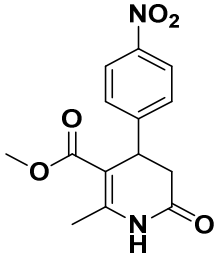	*$C_{14}H_{14}N_2O_5$*	*Off-white*	*202*	*41*
M2	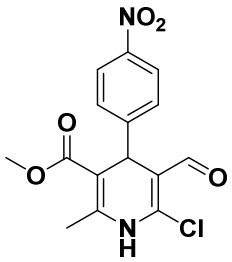	*$C_{15}H_{13}ClN_2O_5$*	Light yellow	*151*	*51.8*

				226–228	
M3	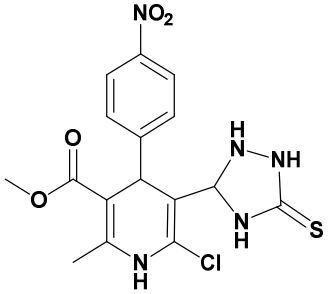	$C_{16}H_{16}ClN_5O_4S$	*Orange*		*50*
M4	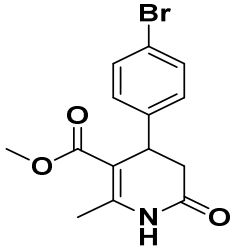	$C_{14}H_{14}BrNO_3$	*Off-white*	*187*	*44.4*
M5	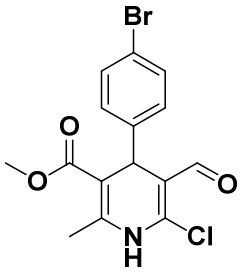	$C_{15}H_{13}BrClNO_3$	Light yellow	*141*	*59.3*
				210–212	
M6	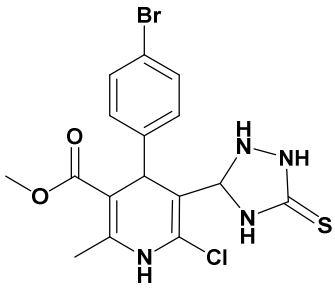	$C_{16}H_{16}BrClN_4O_2S$	*Orange*		*45*
M7	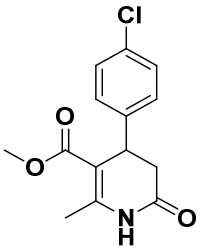	$C_{14}H_{14}ClNO_3$	*Off-white*	*173*	*30*
M8	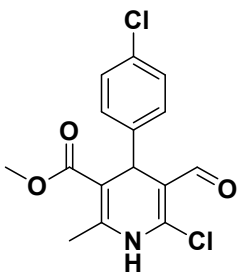	$C_{15}H_{13}Cl_2NO_3$	Light yellow	*136*	*50*

				208–210	
M9	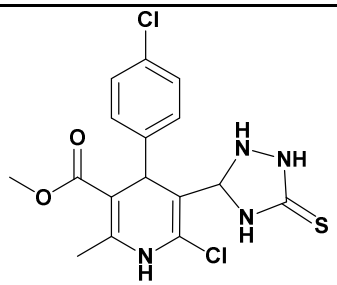	*$C_{16}H_{16}Cl_2N_4O_2S$*	*Orange*		*62.3*
M10	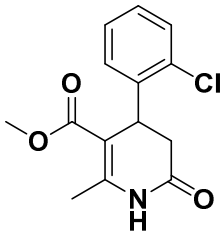	*$C_{14}H_{14}ClNO_3$*	*Off-white*	*195*	*42*
M11	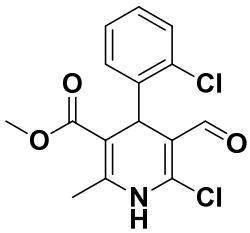	*$C_{15}H_{13}Cl_2NO_3$*	*Yellow*	*190*	*58*
				210–212	
M12	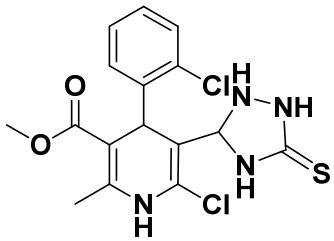	*$C_{16}H_{16}Cl_2N_4O_2S$*	*Orange*		*60*

***Table 2**. Molecular docking scores, RMSD values, and major predicted interactions of osimertinib and compounds M3, M6, M9, and M12 within the EGFR tyrosine kinase active site (PDB ID: 6JWL).*

Compound	GBVI/WSA dG score (kcal/mol)	RMSD (Å)	Ligand atom	Receptor atom/residue	Interaction	Distance (Å)	Interaction energy (kcal/mol)
Osimertinib	-13.8	1.35	—	—	Reference ligand	—	—
M3	−14.4948	2.1930	O (15); S (27)	CE (Lys745); CA (Gly796)	H-acceptor; H-acceptor	3.67; 4.25	−1.3; −0.8
M6	−14.6434	1.4269	O (15)	OG (Thr790)	H-acceptor	3.29	−0.9
M9	−15.9135	2.3085	N (29)	OD2 (Asp855)	H-donor	2.88	−0.8
M12	−14.4427	1.4825	S (27)	NZ (Lys745)	H-acceptor	3.52	−9.5

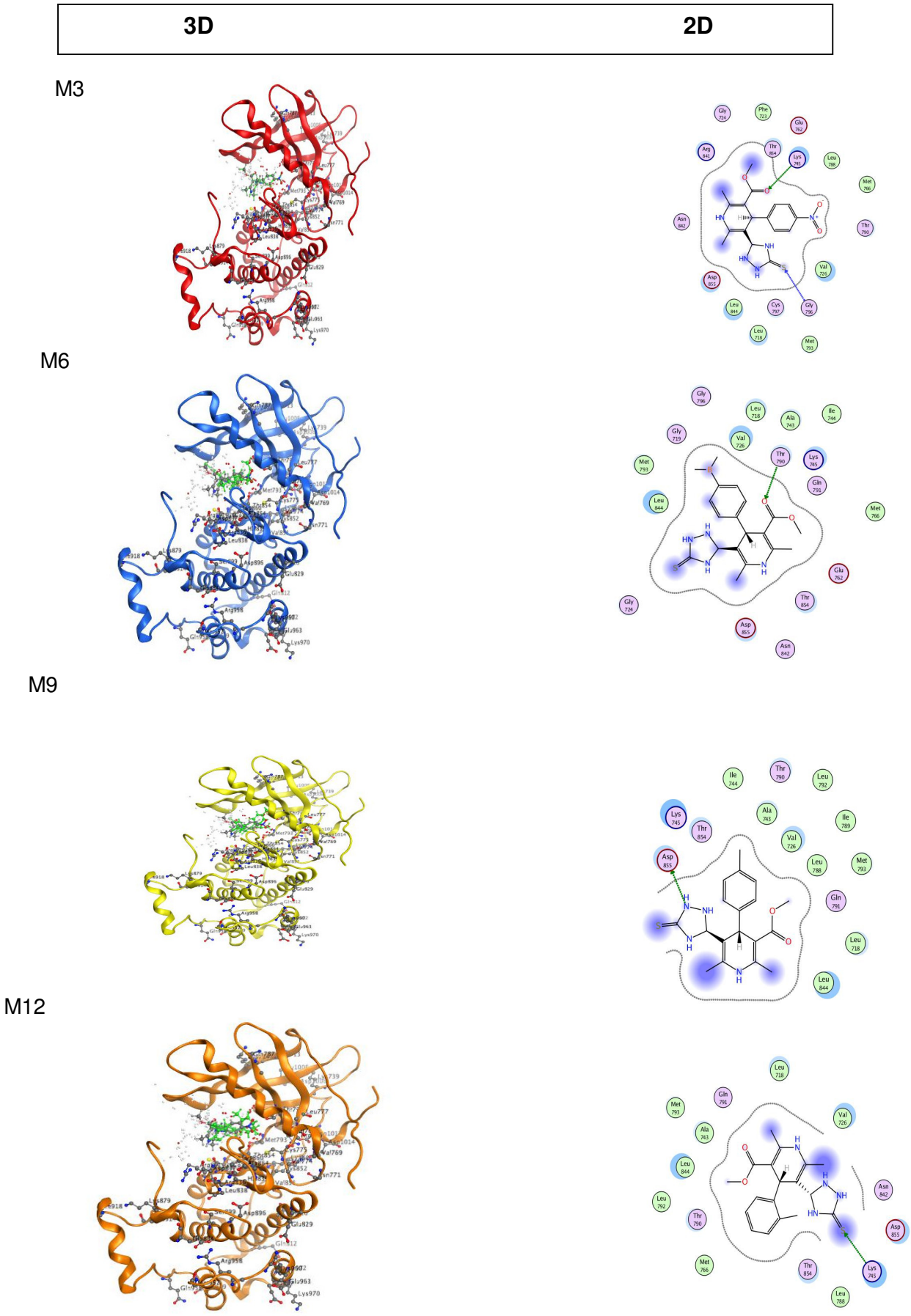

***Figure 13**. Three-dimensional binding poses and two-dimensional interaction diagrams of compounds M3, M6, M9, and M12 within the EGFR tyrosine kinase active site (PDB ID: 6JWL).*

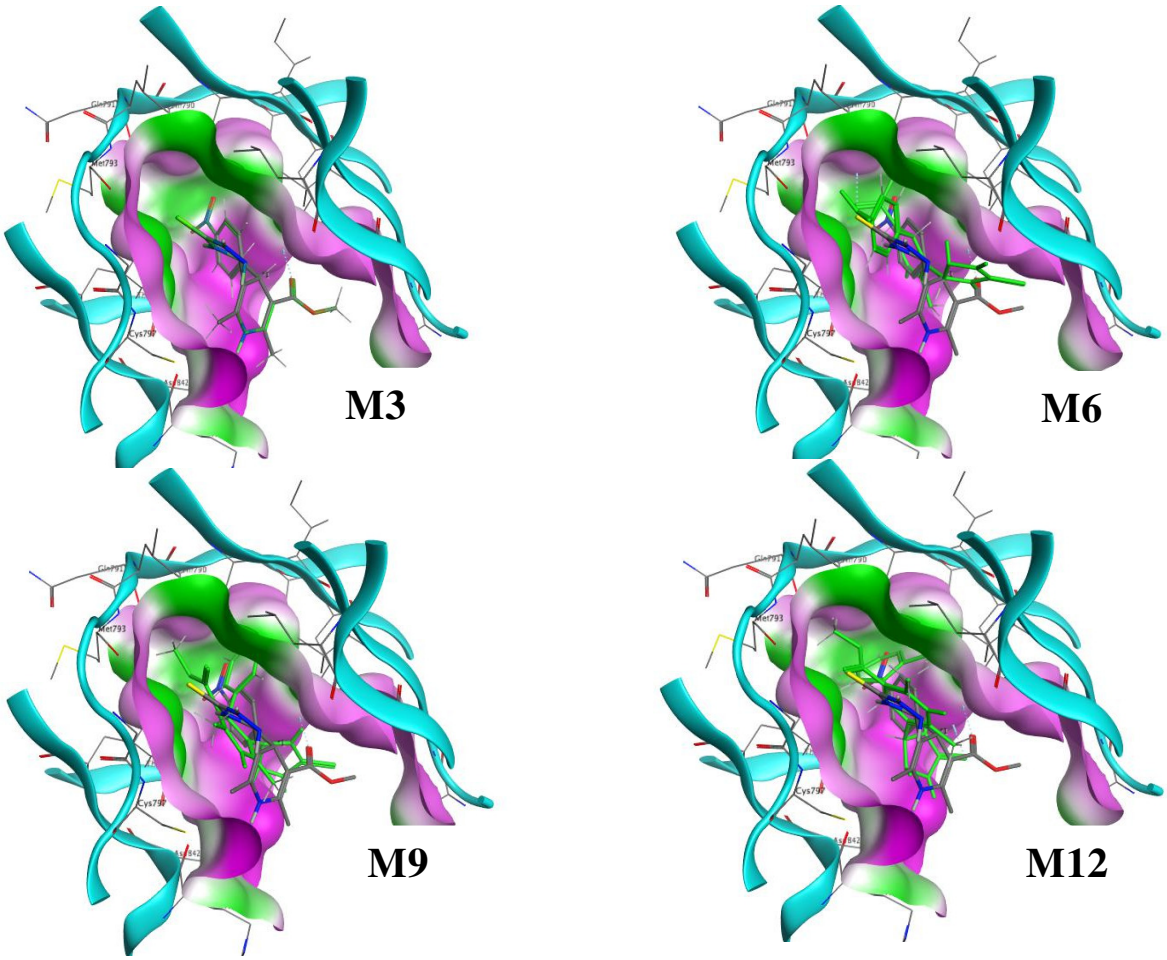

***Figure 14**. Surface representations of compounds M3, M6, M9, and M12 within the EGFR binding pocket, showing their predicted orientations and accommodation within the active site.*

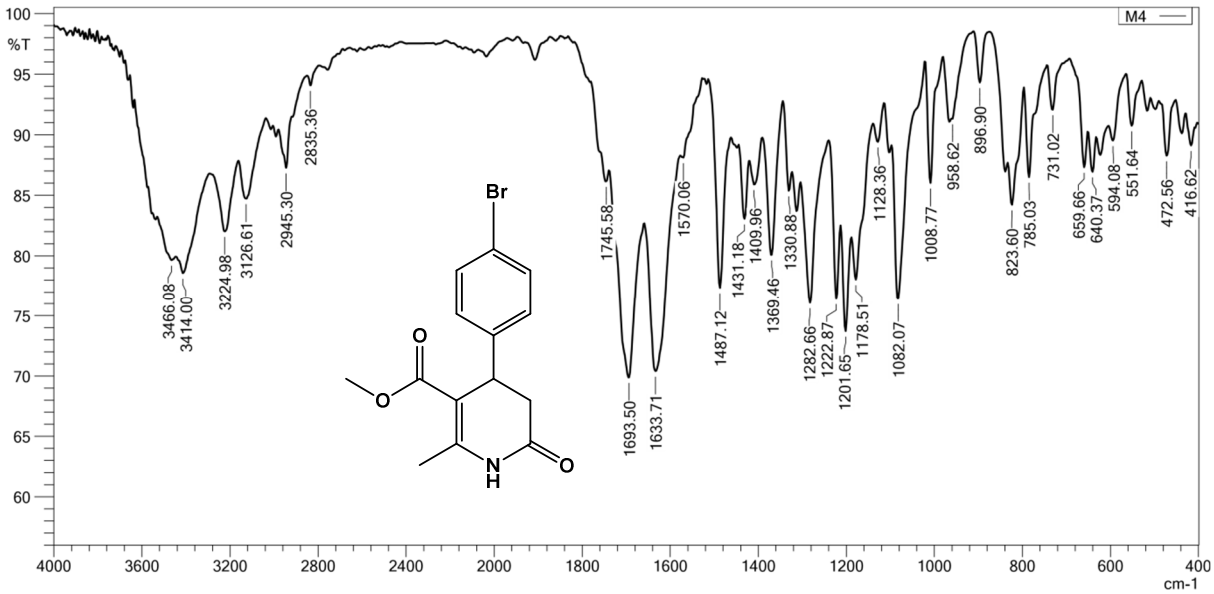

***Figure 15**. FT-IR spectrum of compound M4 (KBr, 4000–400 cm⁻¹).*

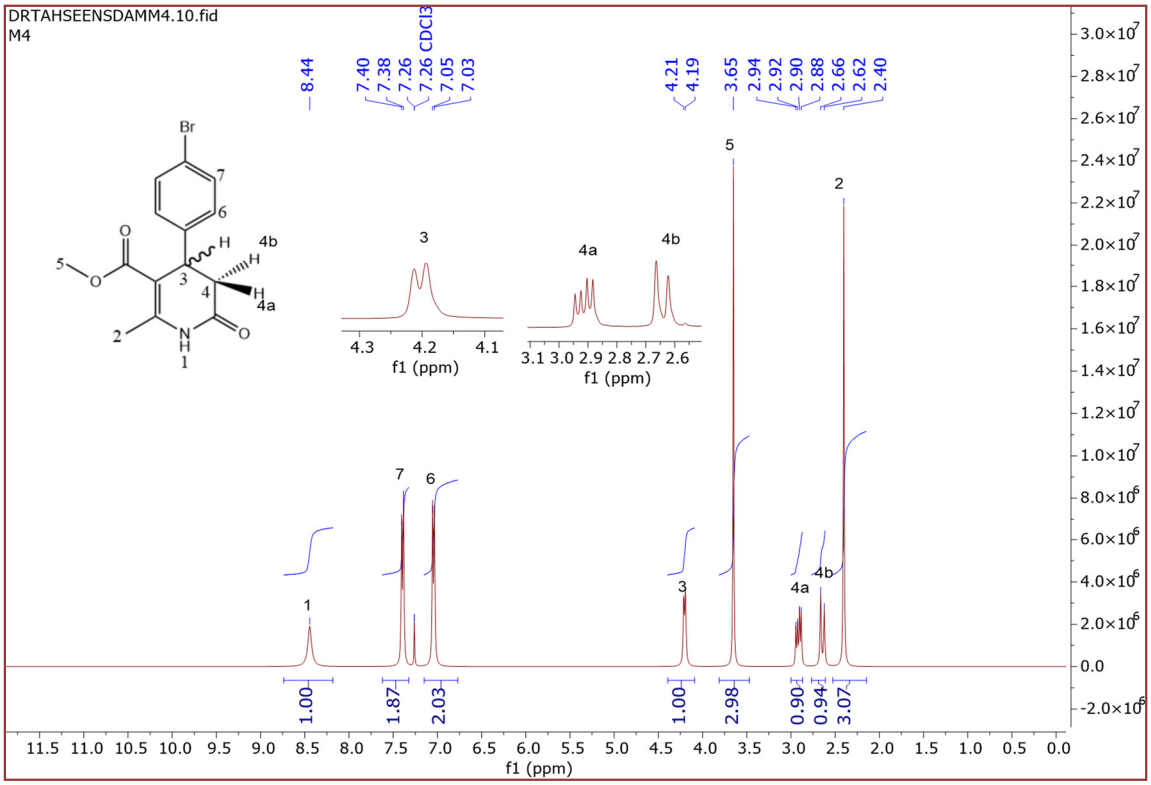

Figure 16. *¹H-NMR spectrum of compound M4 (400 MHz, $CDCl_3$).*

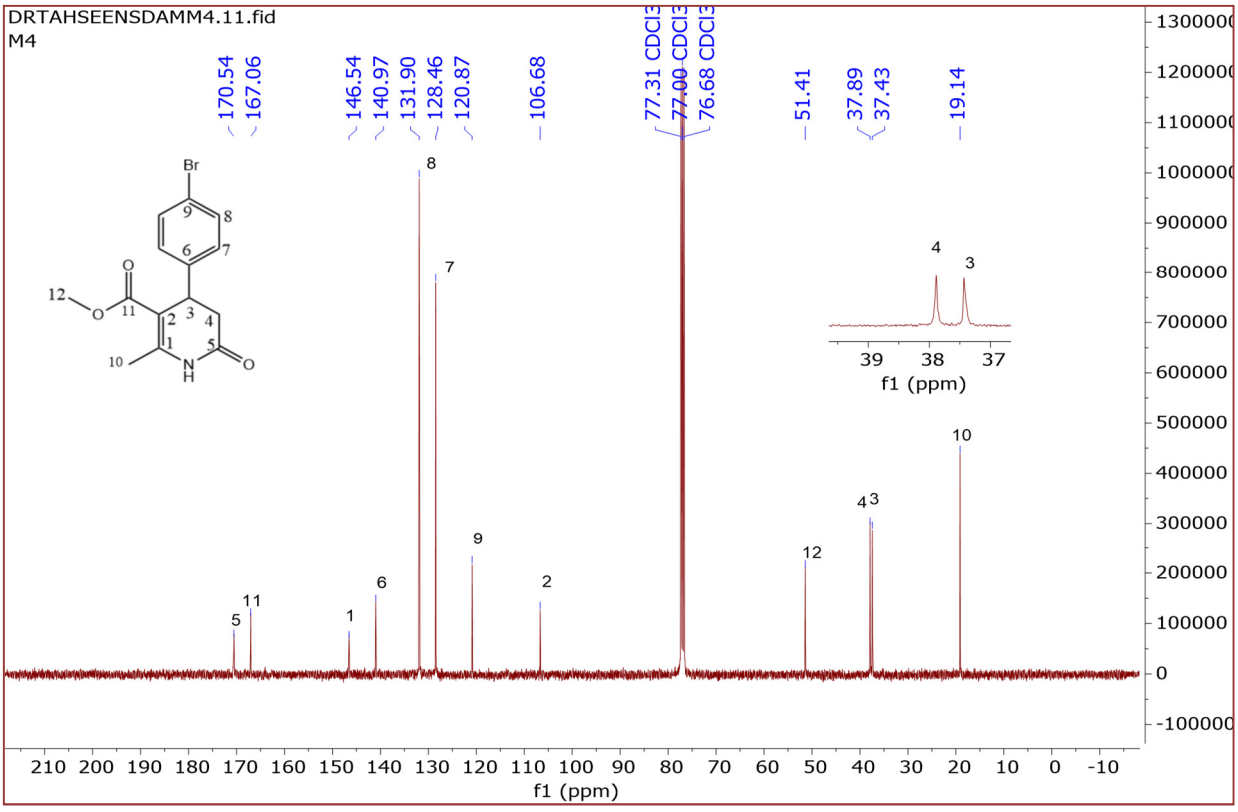

Figure 17. *¹³C-NMR spectrum of compound M4 (101 MHz, $CDCl_3$).*

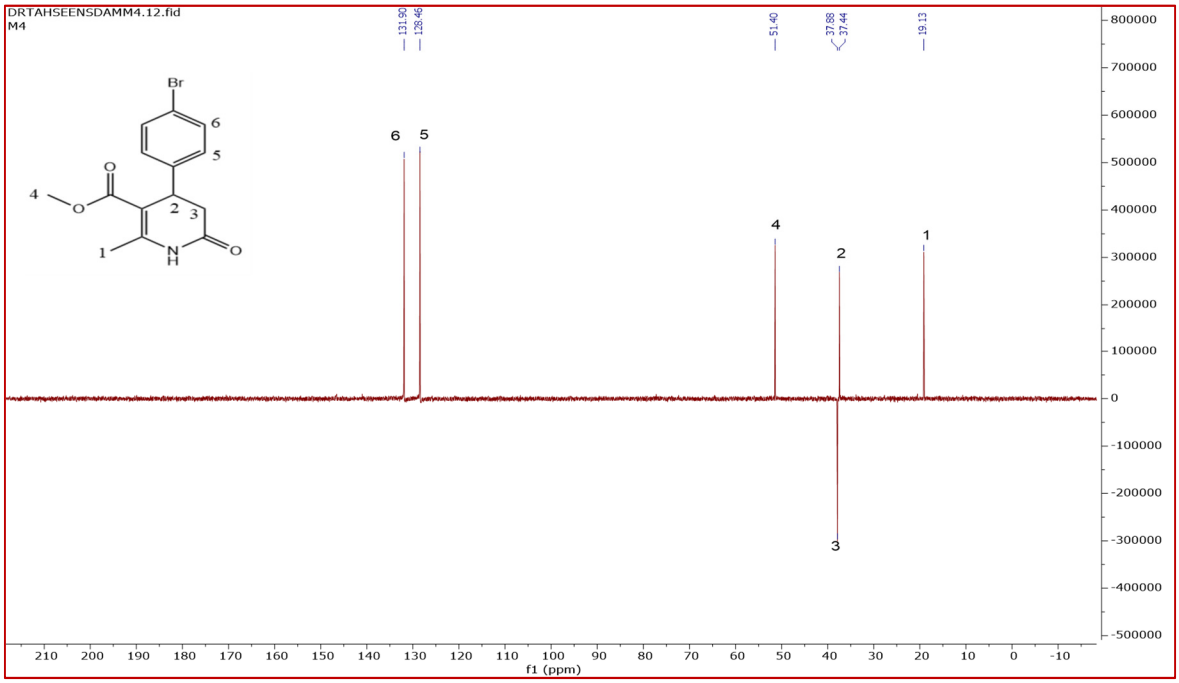

***Figure 18**. DEPT-135 spectrum of compound M4.*

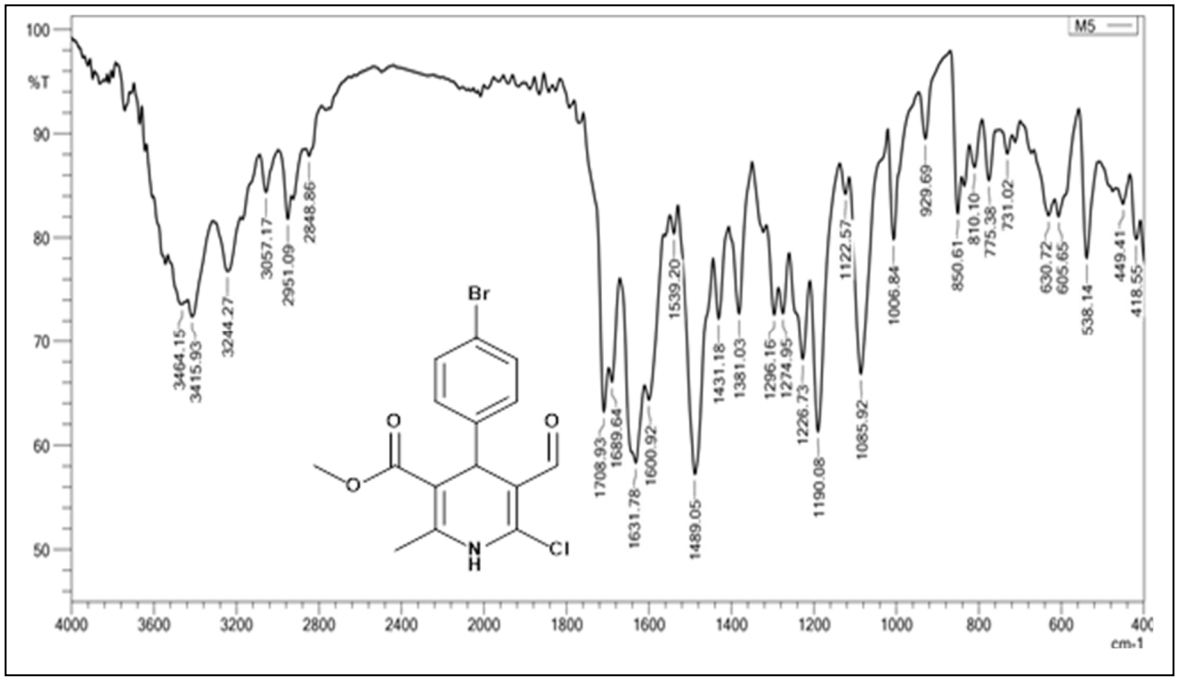

***Figure 19**. FT-IR spectrum of compound M5 (KBr, 4000–400 cm⁻¹).*

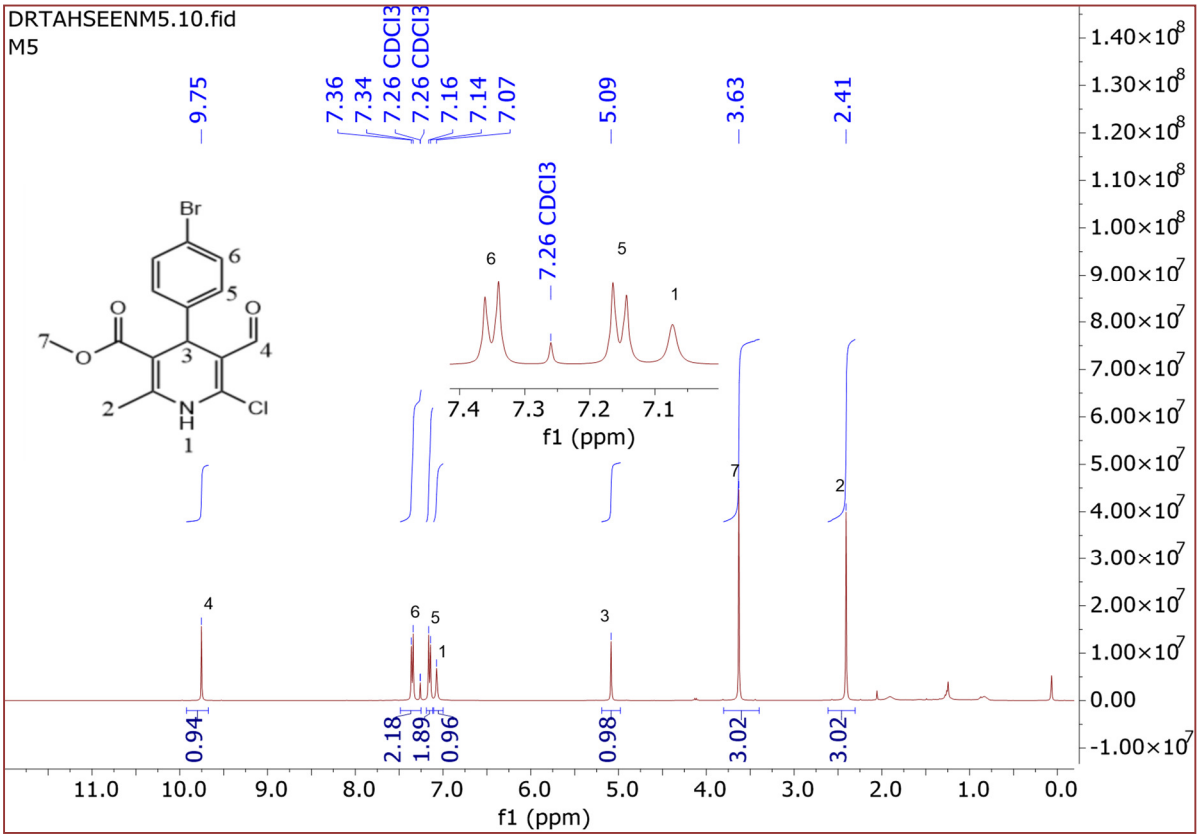

Figure 20. *[1]H-NMR spectrum of compound M5 (400 MHz, $CDCl_3$).*

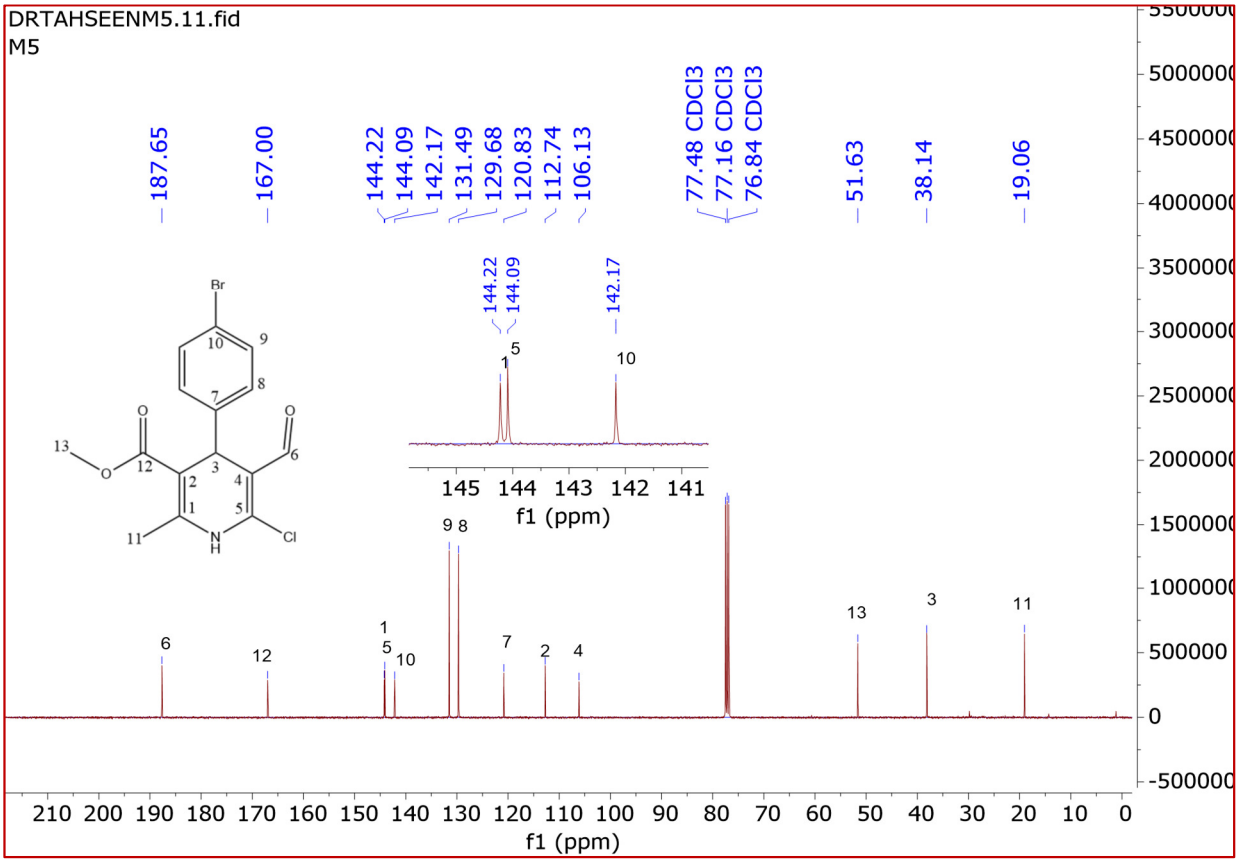

Figure 21. *[13]C-NMR spectrum of compound M5 (101 MHz, $CDCl_3$).*

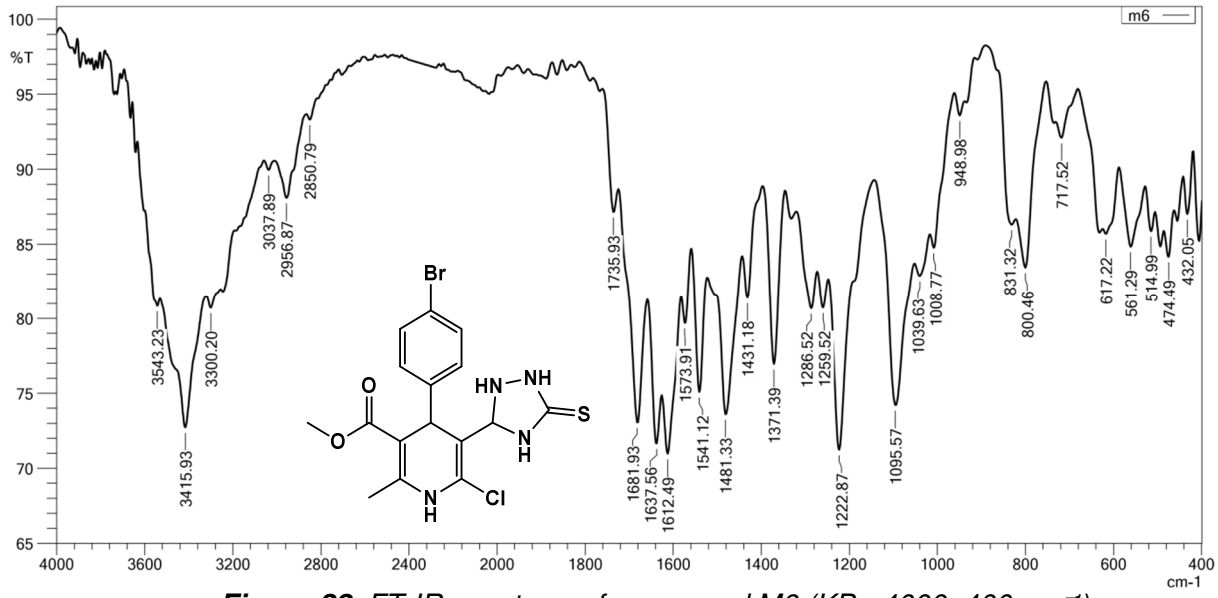

***Figure 22**. FT-IR spectrum of compound M6 (KBr, 4000–400 cm⁻¹).*

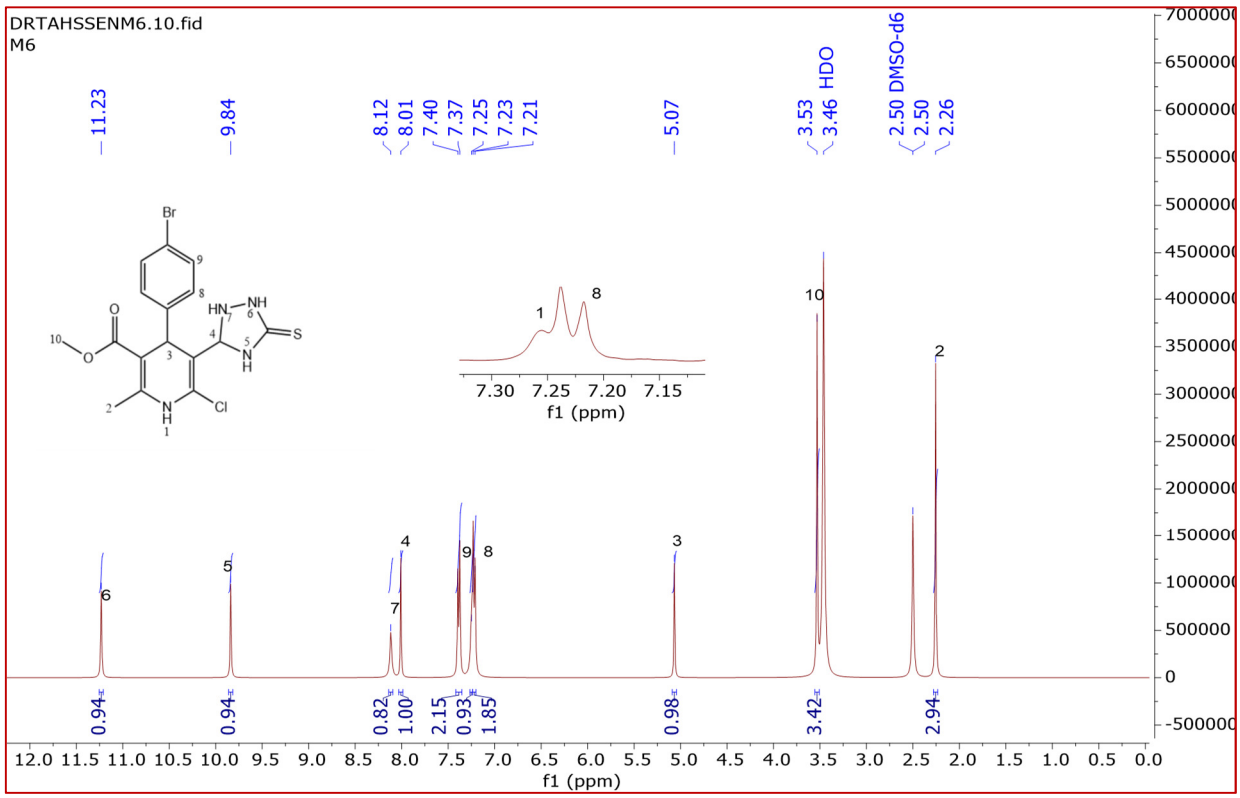

***Figure 23**. ¹H-NMR spectrum of compound M6 (400 MHz, DMSO-d_6).*

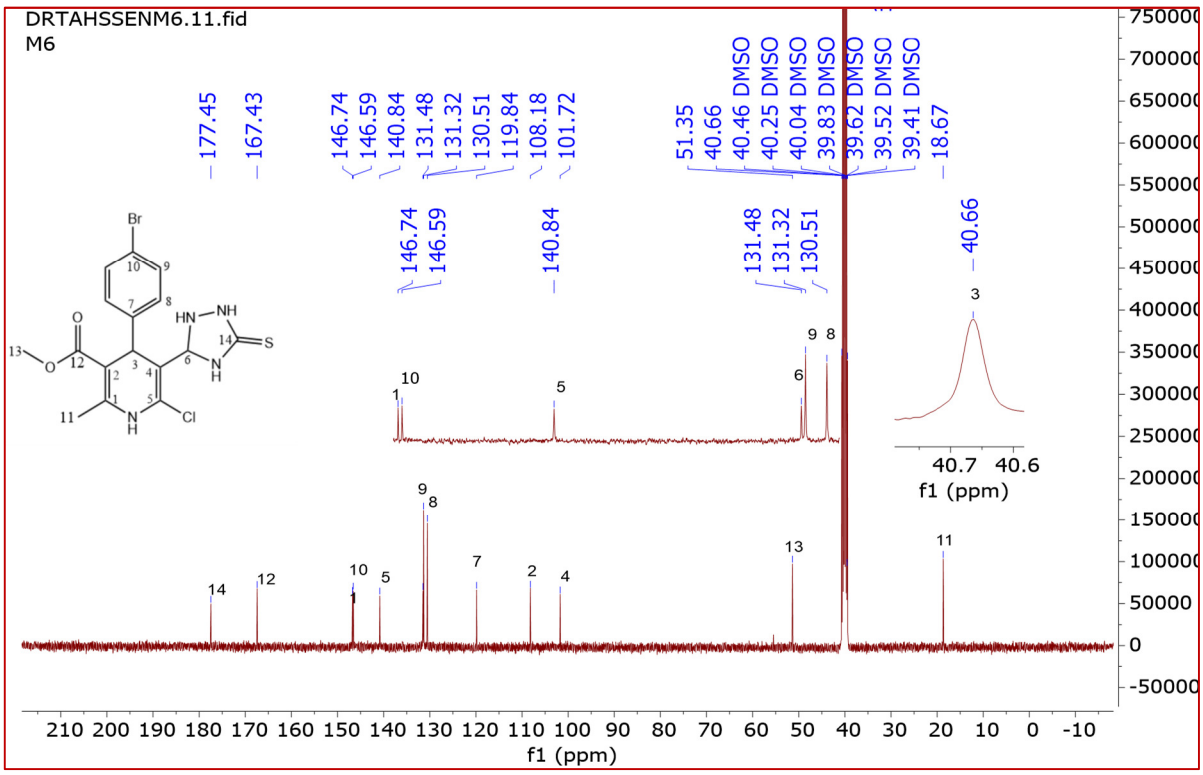

Figure 24. *^{13}C-NMR spectrum of compound M6 (101 MHz, DMSO-d_6).*

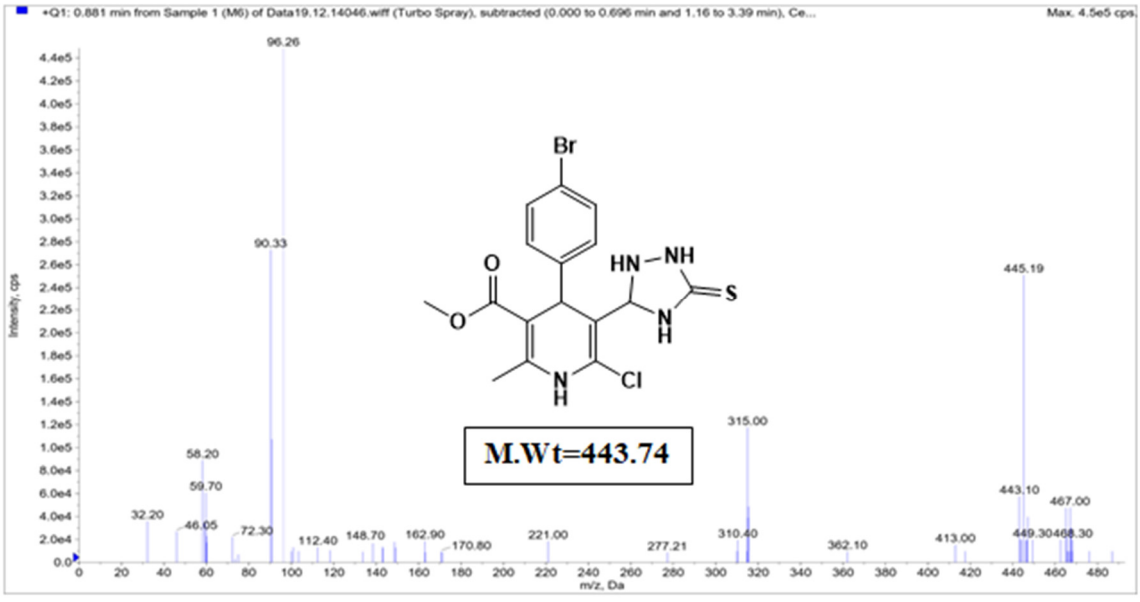

Figure 25. *ESI mass spectrum of compound M6.*

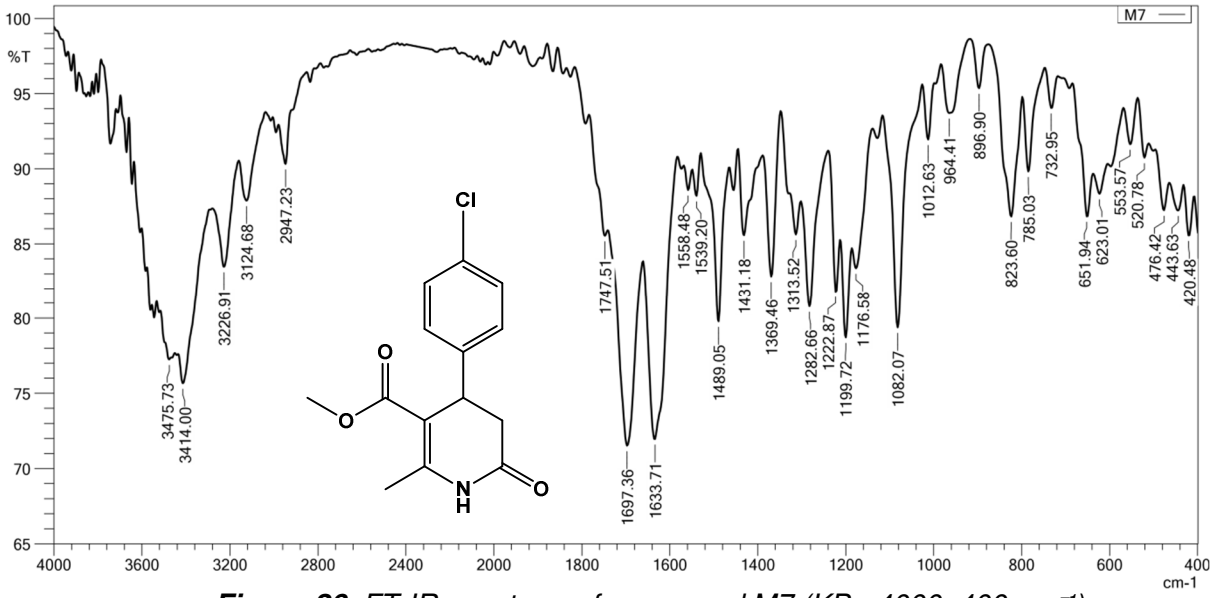

***Figure 26**. FT-IR spectrum of compound M7 (KBr, 4000–400 cm⁻¹).*

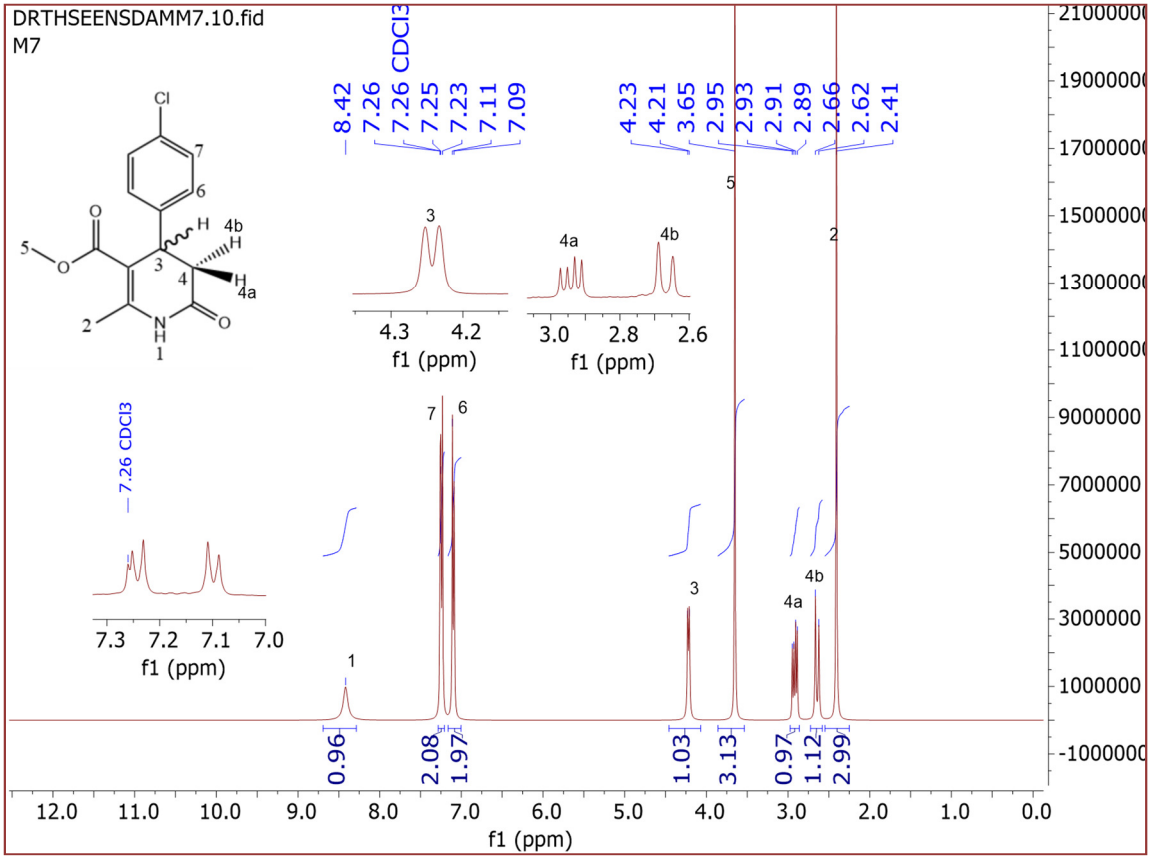

***Figure 27**. ¹H-NMR spectrum of compound M7 (400 MHz, $CDCl_3$).*

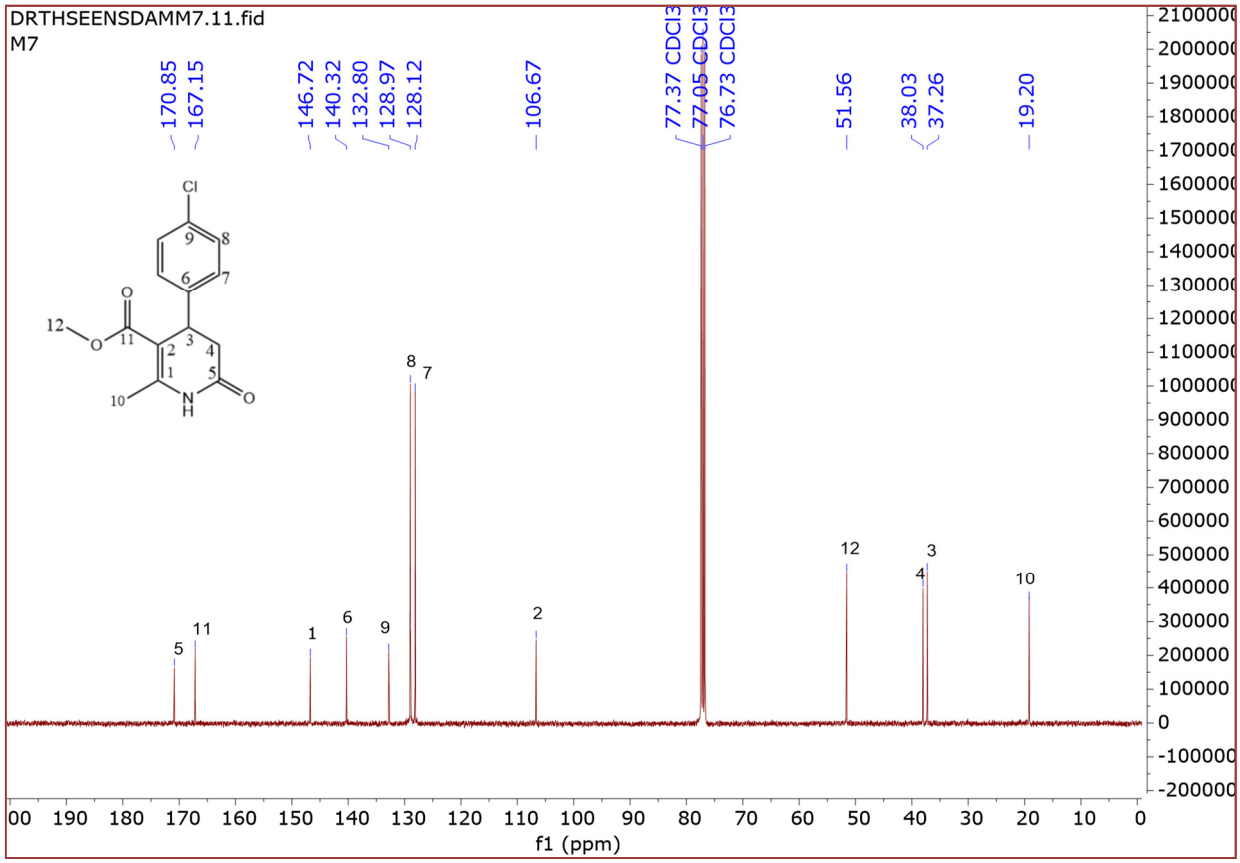

Figure 28. *^{13}C-NMR spectrum of compound M7 (101 MHz, $CDCl_3$).*

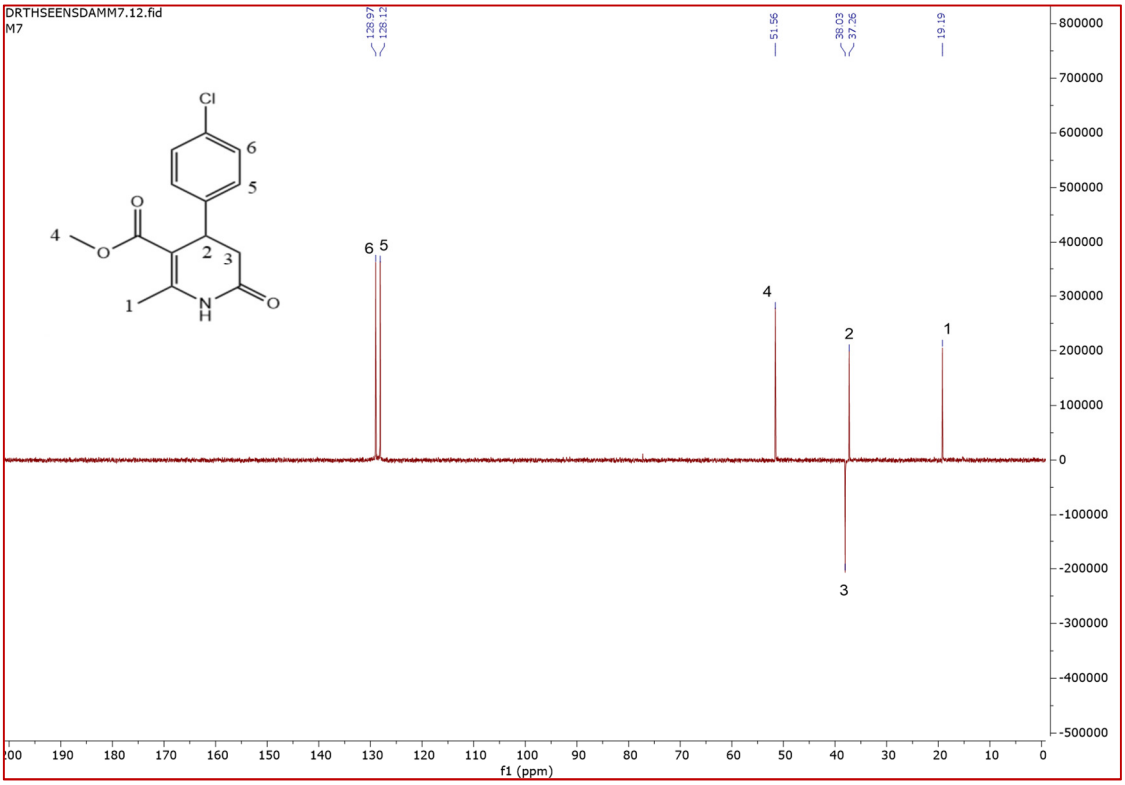

Figure 29. *DEPT-135 spectrum of compound M7.*

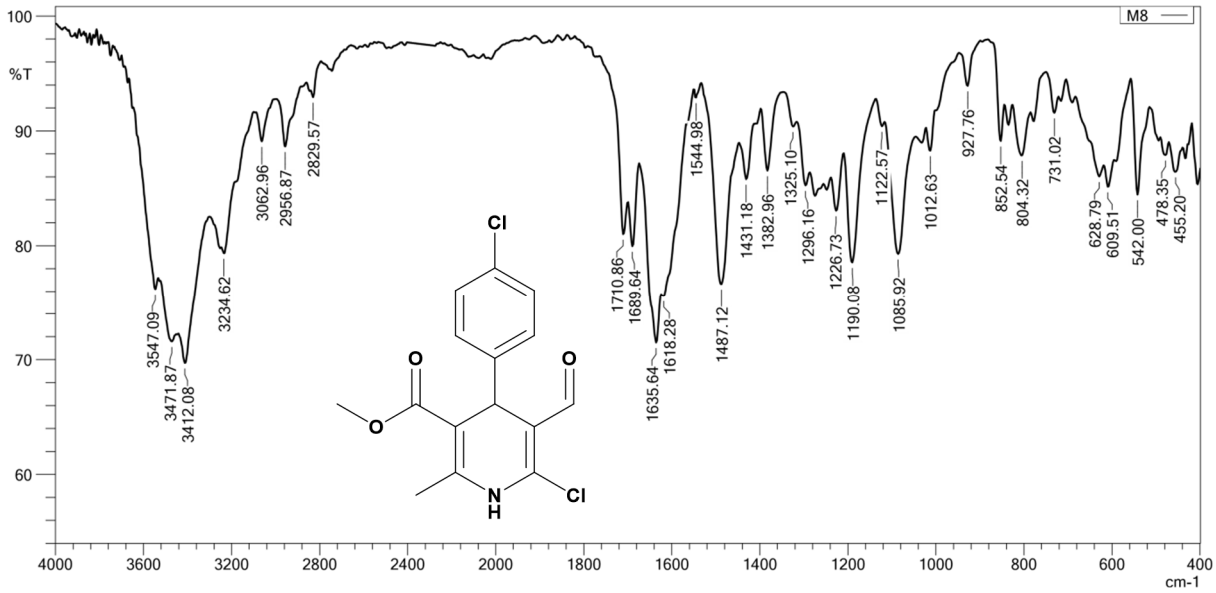

Figure 30. *FT-IR spectrum of compound M8 (KBr, 4000–400 cm⁻¹).*

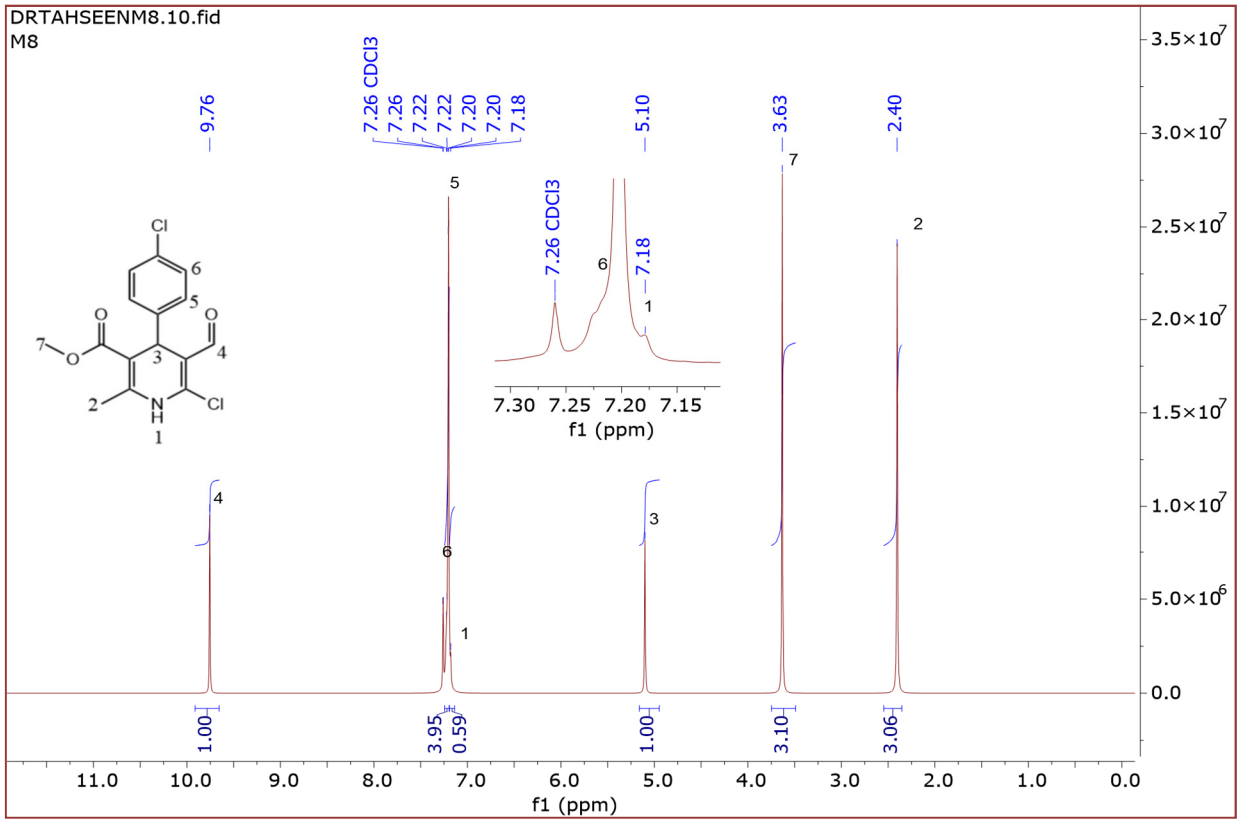

Figure 31. *¹H-NMR spectrum of compound M8 (400 MHz, $CDCl_3$).*

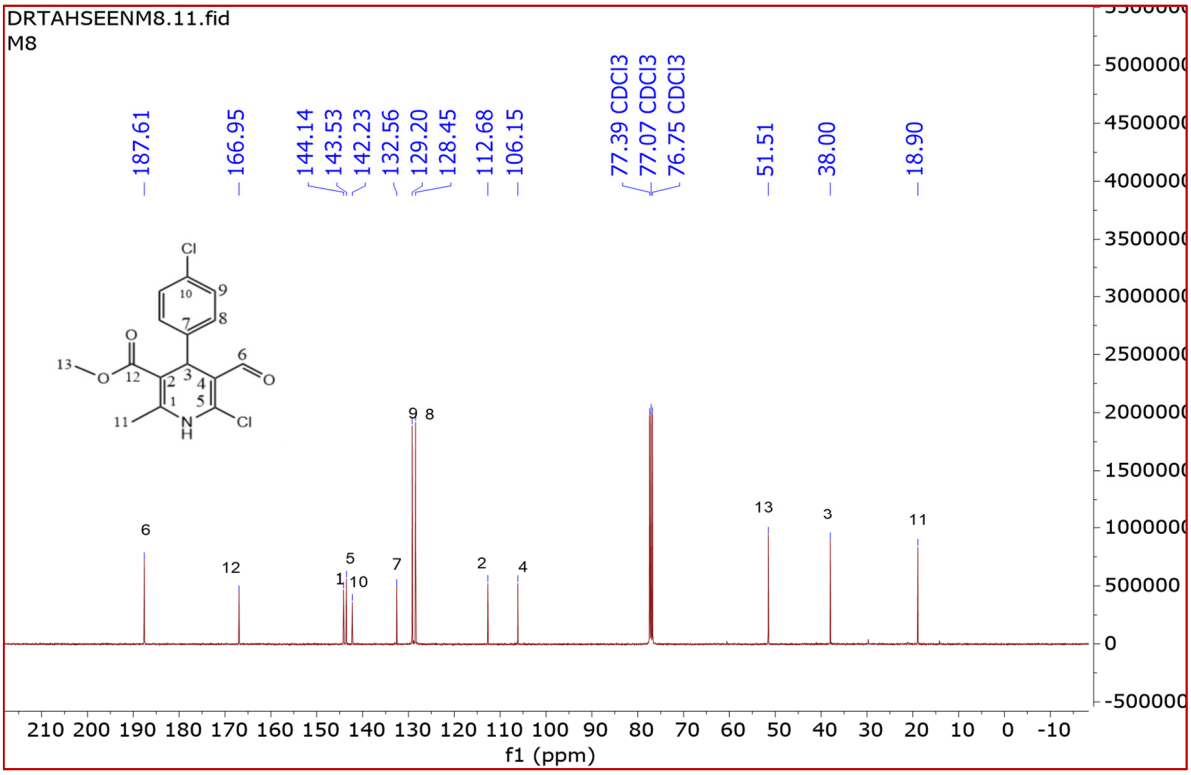

Figure 32. *^{13}C-NMR spectrum of compound M8 (101 MHz, $CDCl_3$).*

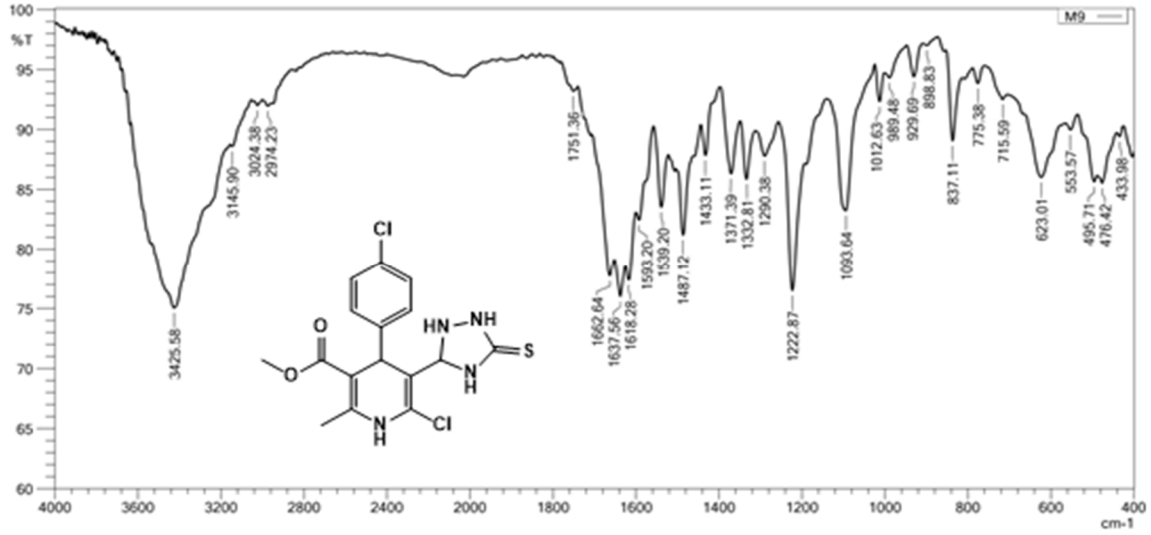

Figure 33. *FT-IR spectrum of compound M9 (KBr, 4000–400 cm^{-1}).*

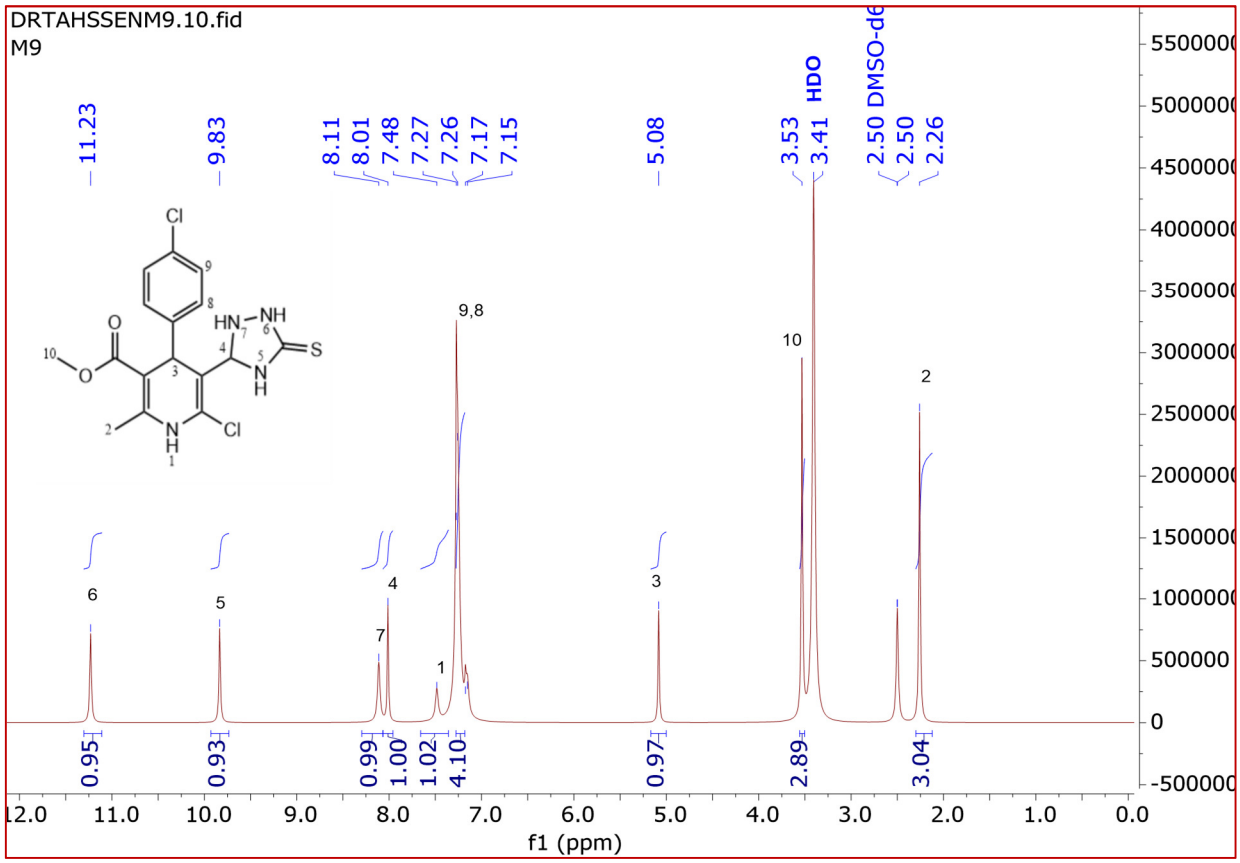

Figure 34. *¹H-NMR spectrum of compound M9 (400 MHz, DMSO-d_6).*

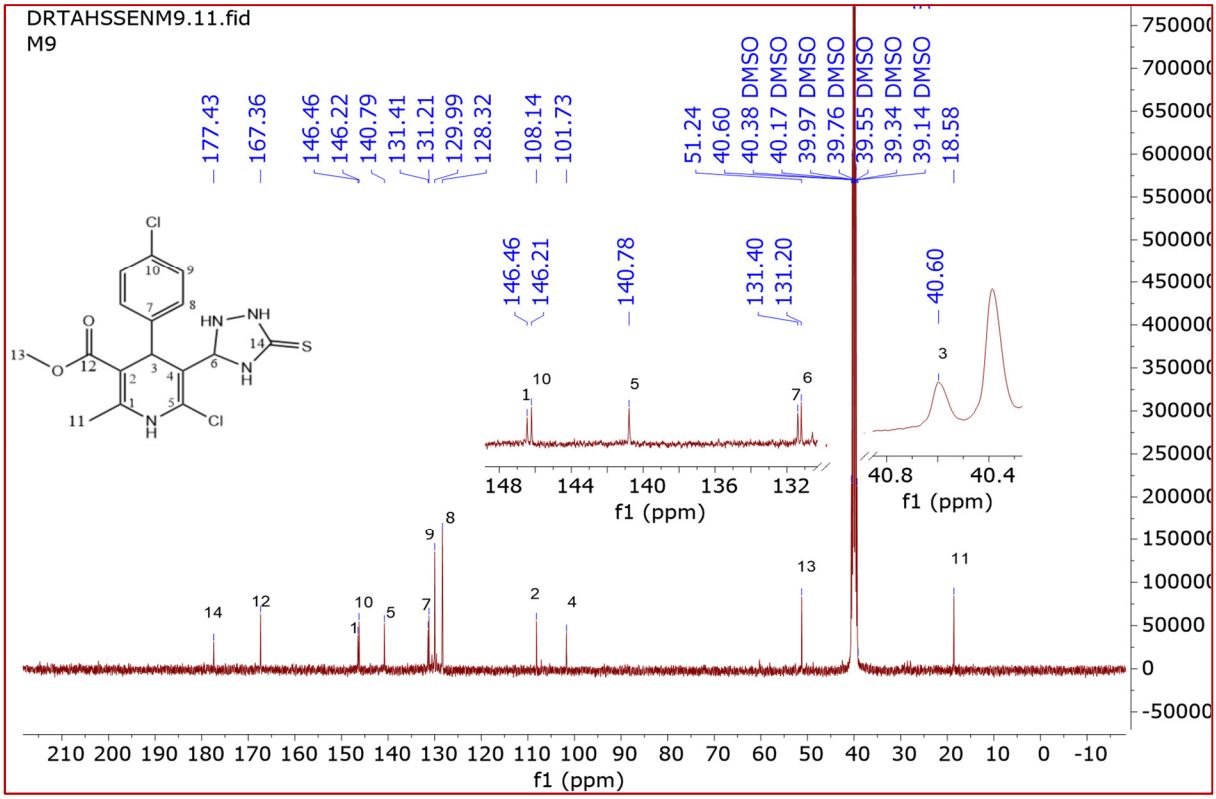

Figure 35. *¹³C-NMR spectrum of compound M9 (101 MHz, DMSO-d_6).*

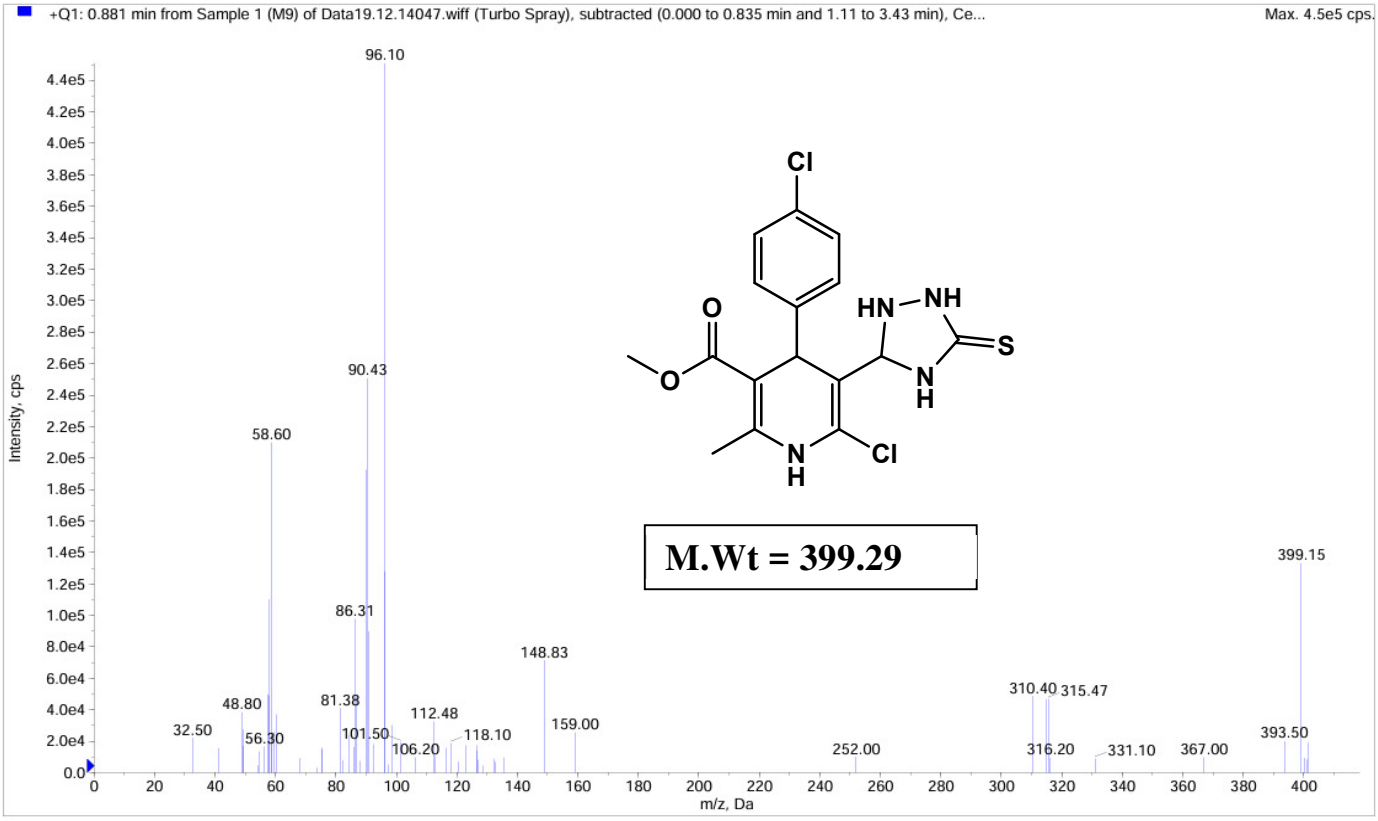

***Figure 36**. ESI mass spectrum of compound M9.*

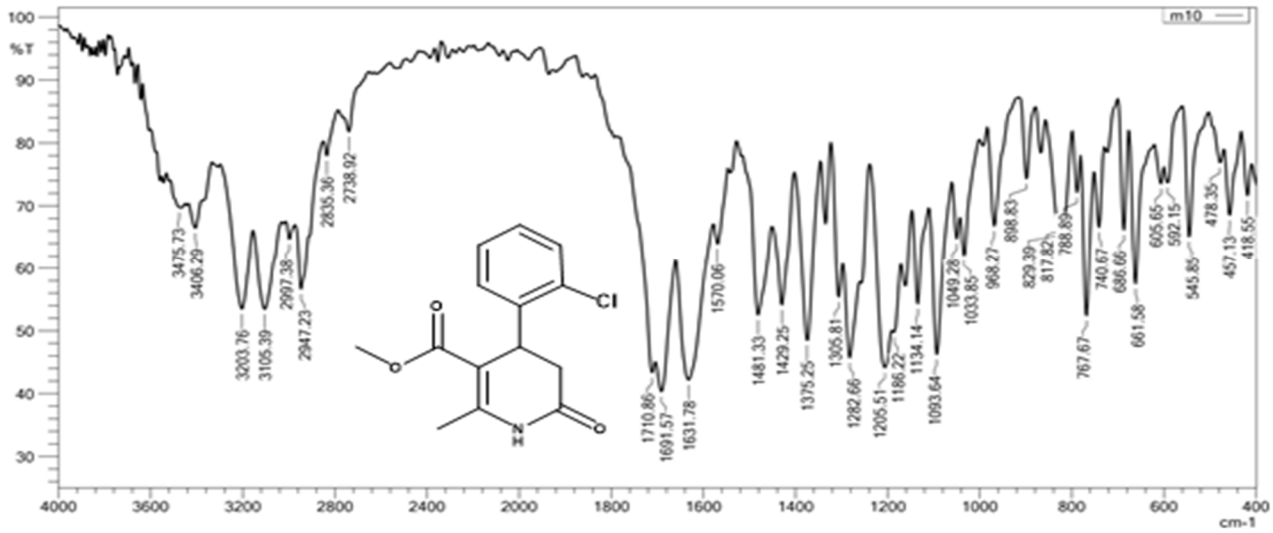

***Figure 37**. FT-IR spectrum of compound M10 (KBr, 4000–400 cm⁻¹).*

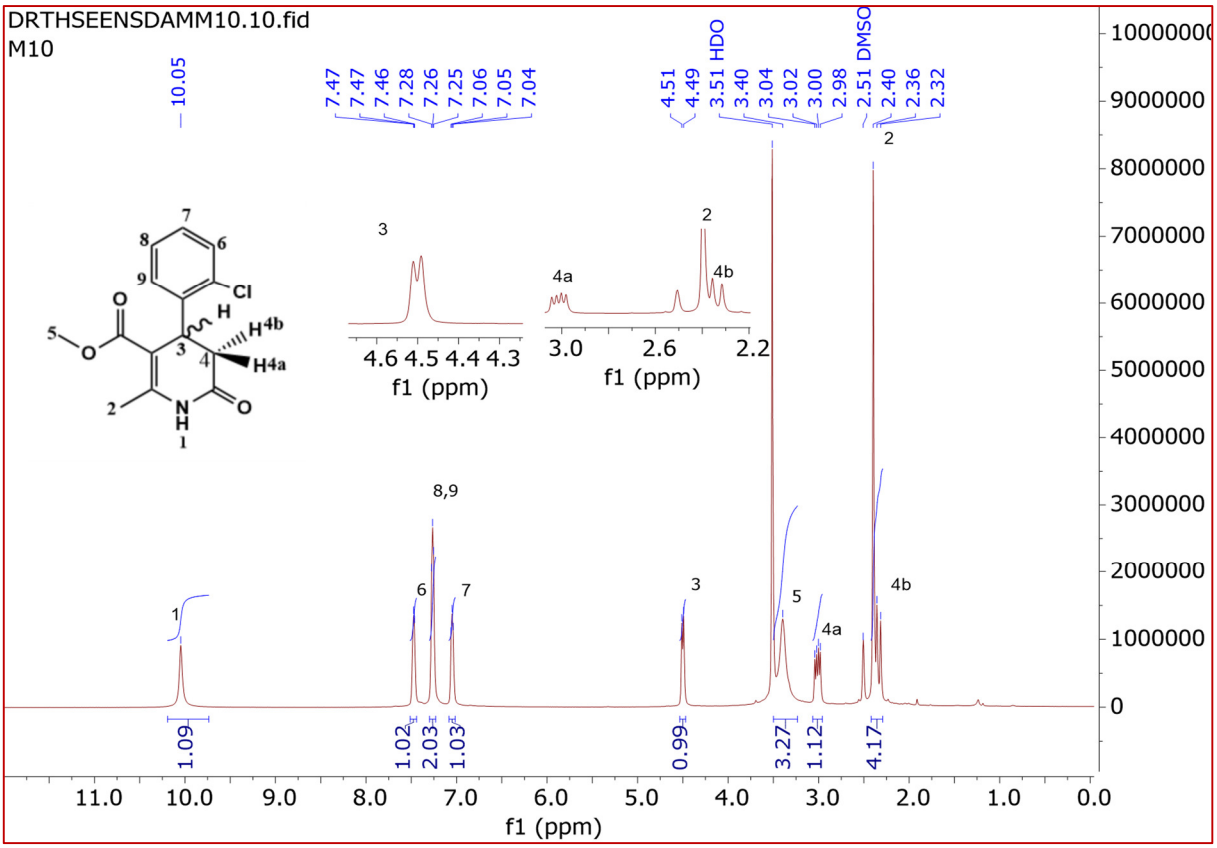

Figure 38. *[1]H-NMR spectrum of compound M10 (400 MHz, DMSO-d_6).*

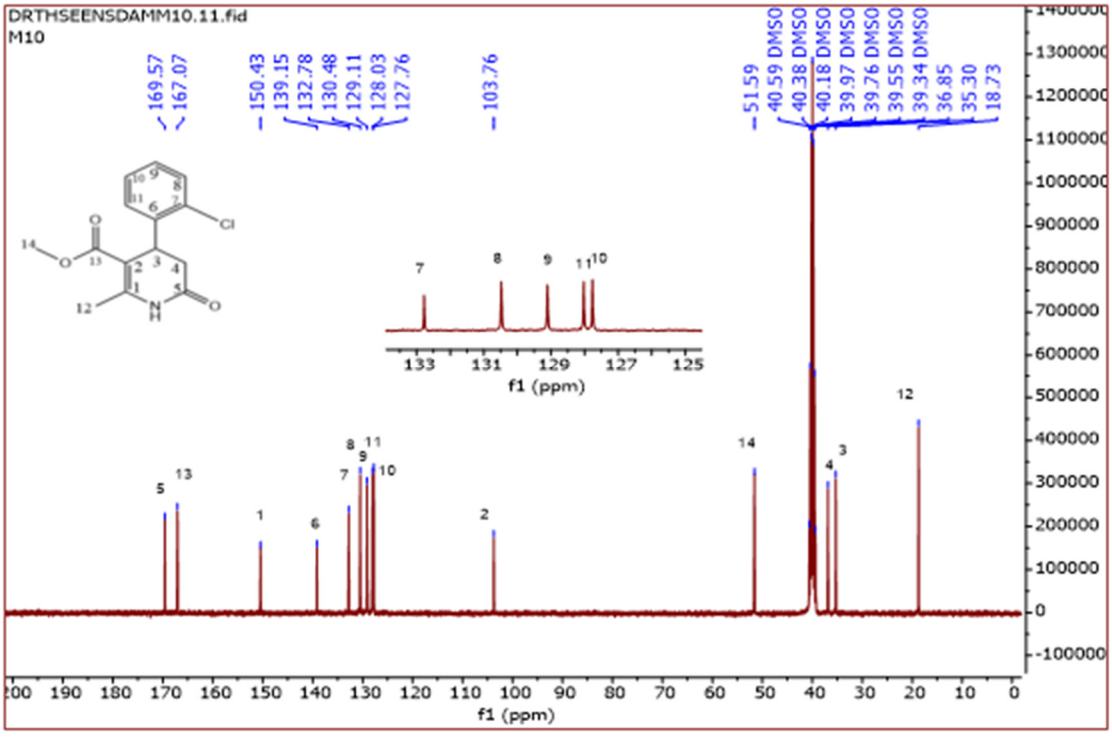

Figure 39. *[13]C-NMR spectrum of compound M10 (101 MHz, DMSO-d_6).*

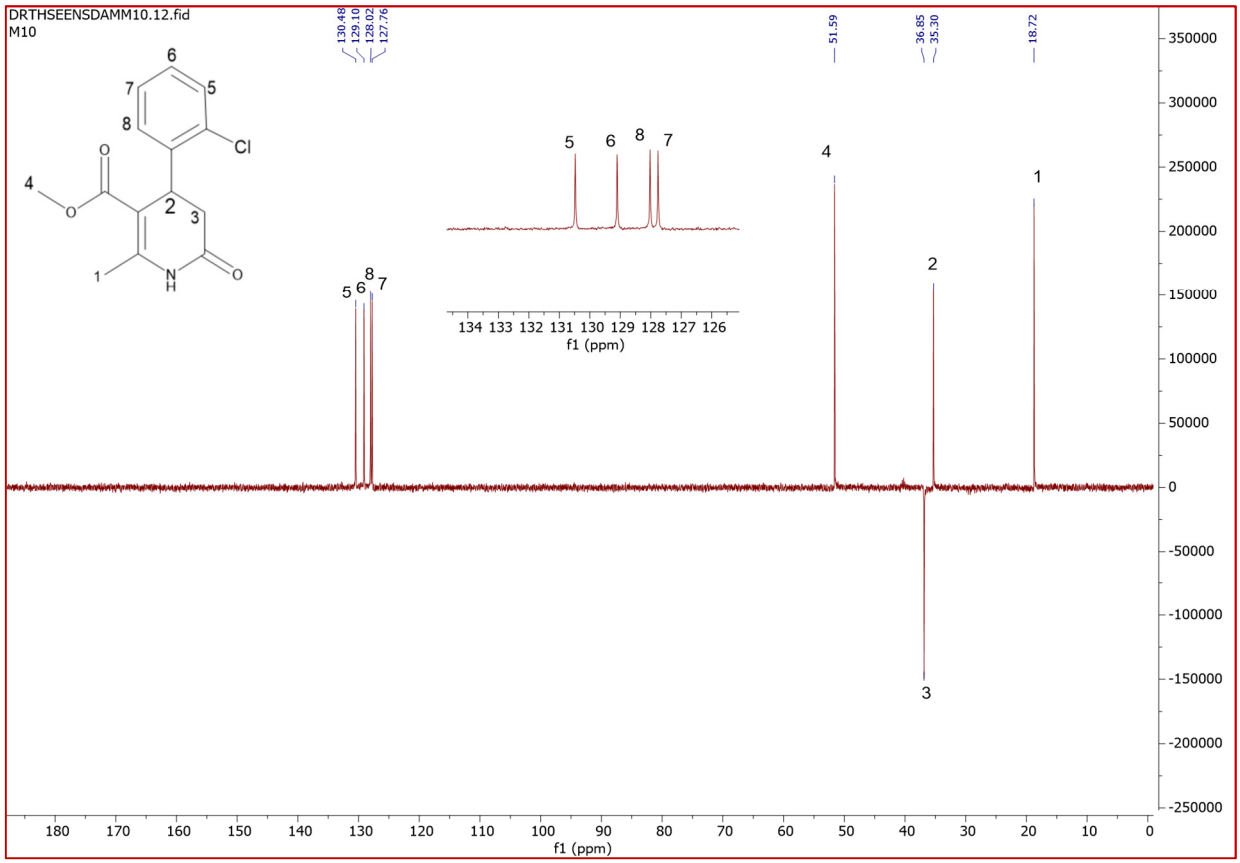

***Figure 40**. DEPT-135 spectrum of compound M10.*

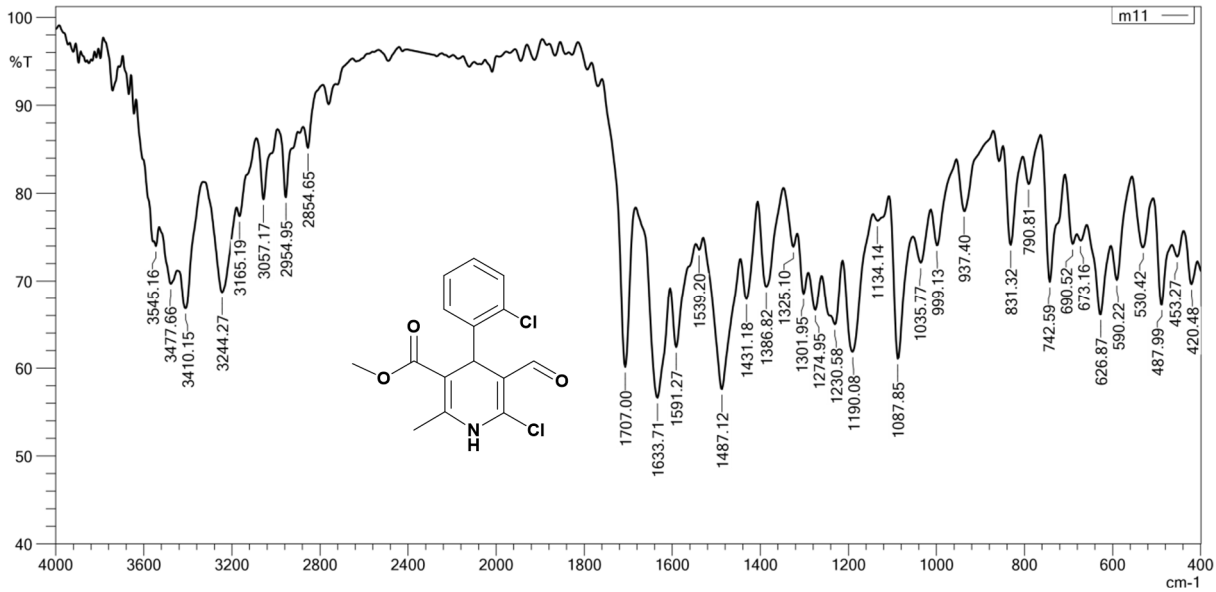

***Figure 41**. FT-IR spectrum of compound M11 (KBr, 4000–400 cm⁻¹).*

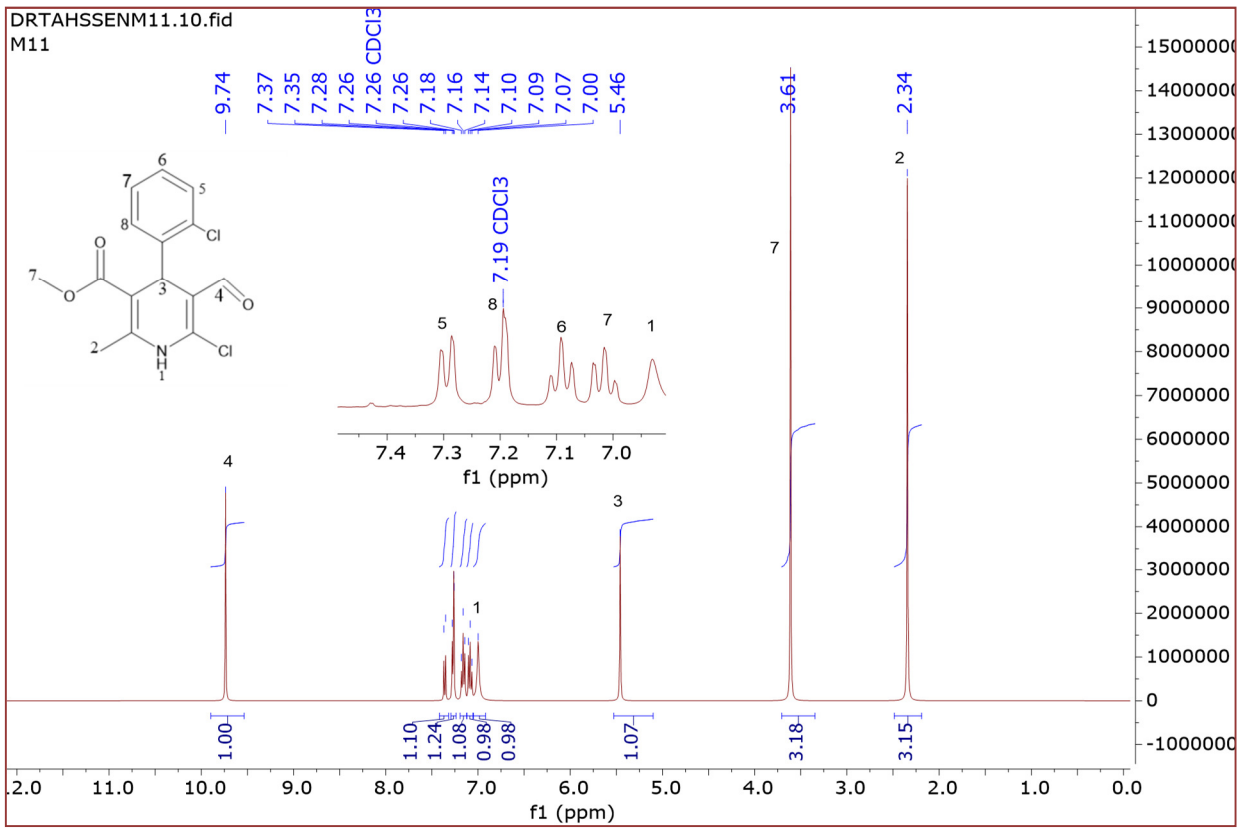

Figure 42. *¹H-NMR spectrum of compound M11 (400 MHz, $CDCl_3$).*

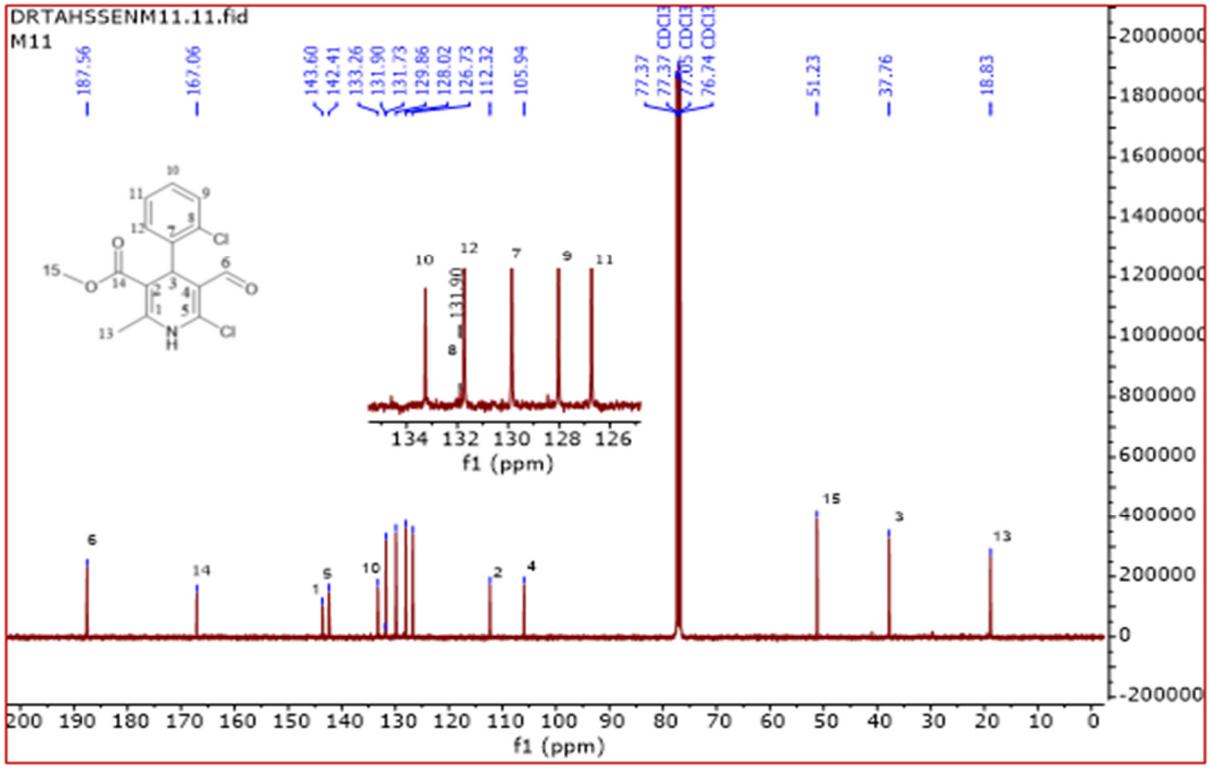

Figure 43. *¹³C-NMR spectrum of compound M11 (101 MHz, $CDCl_3$).*

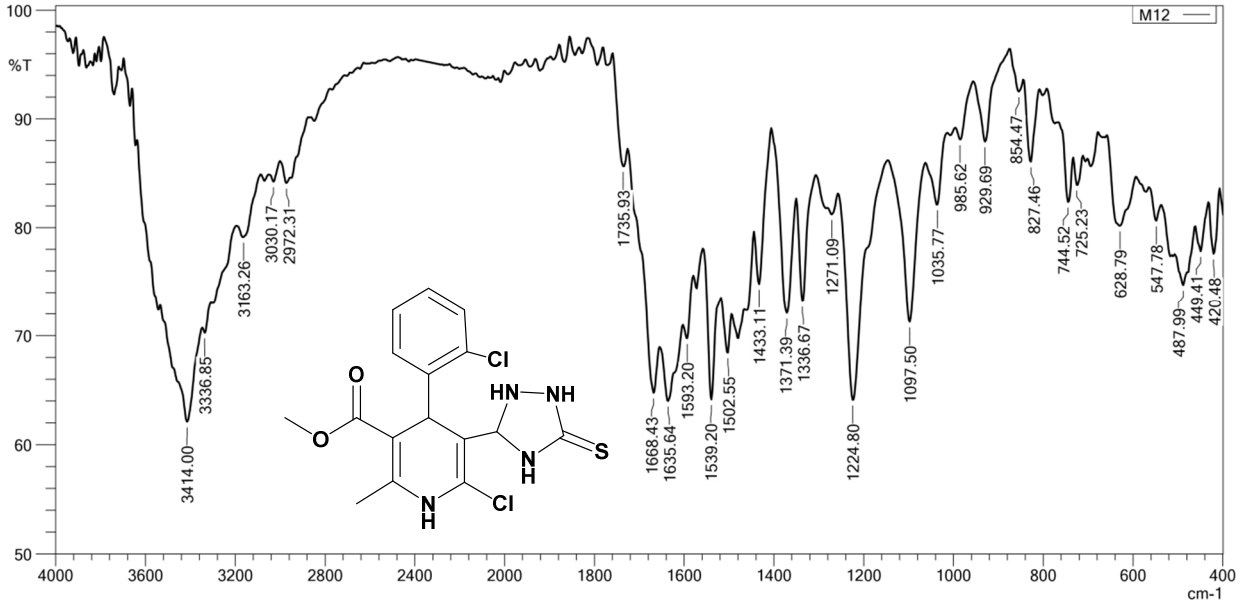

Figure 44. *FT-IR spectrum of compound M12 (KBr, 4000–400 cm⁻¹).*

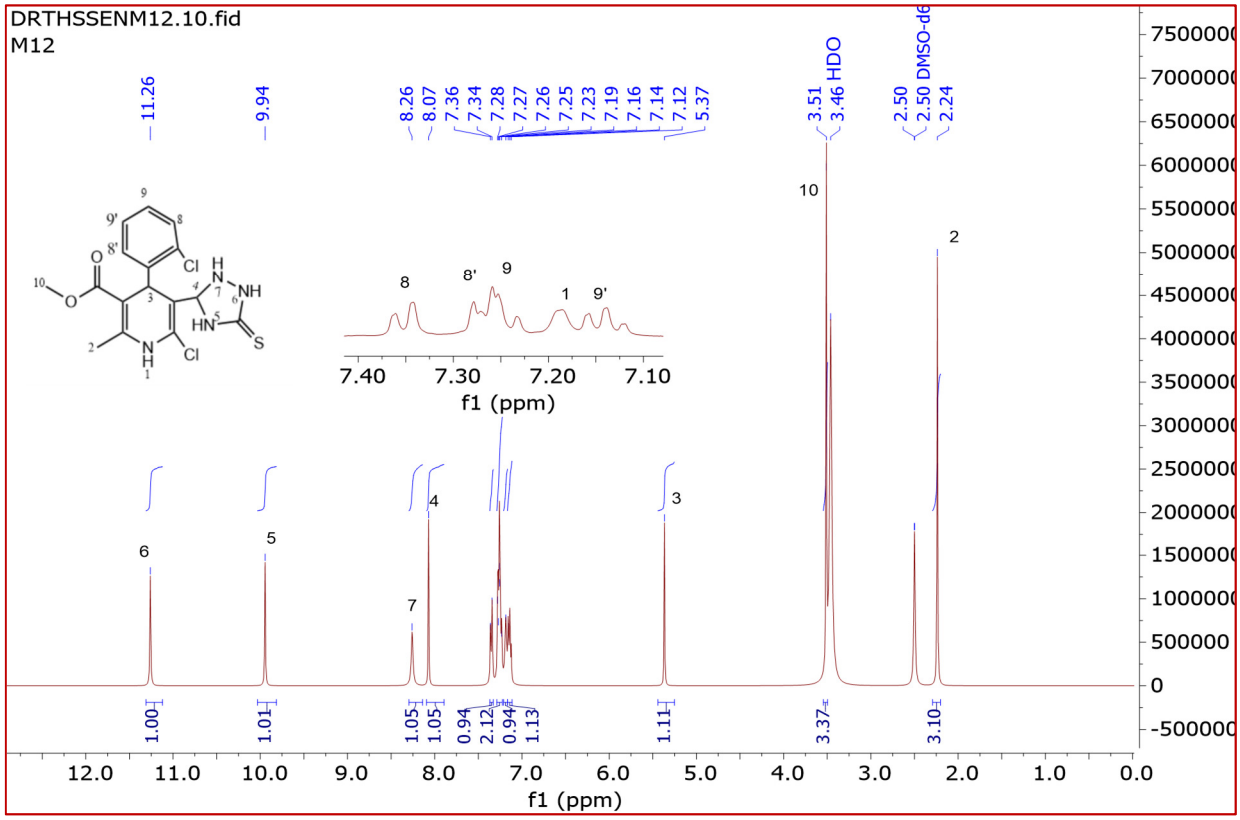

Figure 45. *¹H-NMR spectrum of compound M12 (400 MHz, DMSO-d_6).*

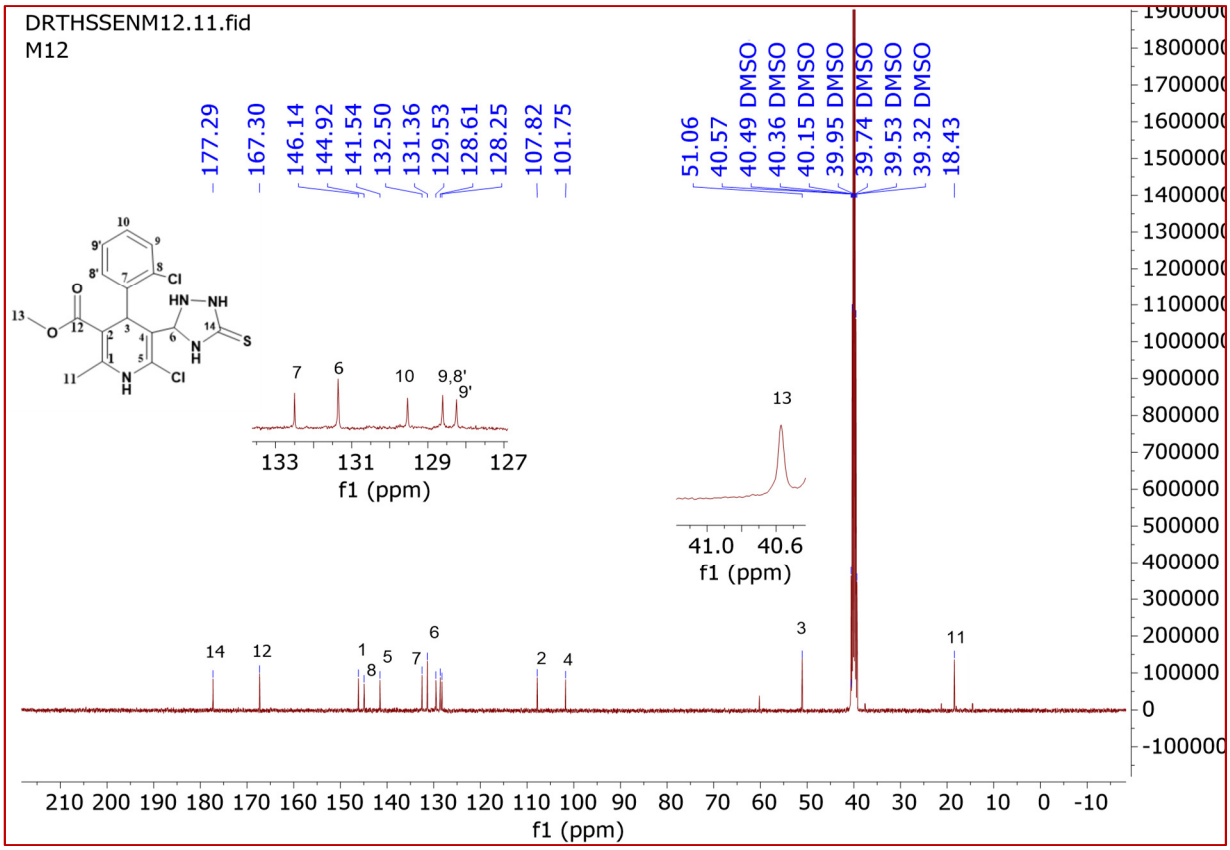

Figure 46. *^{13}C-NMR spectrum of compound M12 (101 MHz, DMSO-d_6).*